

Temporal-Smoothed Incremental Heuristic Dynamic Programming for Cascaded Online Learning Flight Control System

Yifei Li, Erik-Jan van Kampen

Abstract

Model-free reinforcement learning has demonstrated the capability to adjust control laws using data-constructed policy gradients. Its application to online flight control commonly adopts a cascaded control architecture, which enables efficient policy learning for angle-of-attack tracking using control-surface deflections. However, the tracking performance and system stability are degraded by oscillatory actions. To address this issue, we incorporate policy regularization for temporal action smoothness and a low-pass filter to attenuate both the amplitude and oscillatory frequency of actions. The Fast Fourier Transform (FFT) algorithm is used to analyze action smoothness in the frequency-domain representation. Flight control simulations demonstrate the effectiveness of the two proposed techniques.

Index Terms

reinforcement learning, symmetry, data augmentation, approximate value iteration, flight control.

I. INTRODUCTION

Model-free reinforcement learning (RL) has been applied to flight control law optimization without using an accurate system model for state prediction. This approach significantly reduce the effort required to model the complex dynamics of aerial vehicles in control design, as the policy gradient is constructed using measured data. The ADP-based implementation of model-free RL does not require learning a full system model, since only the first-order derivatives of the system dynamics are needed to construct the policy gradients. This motivates the use of a simpler model with fewer parameters than an artificial neural network, which is commonly used in various ADP methods, while still capturing the required first-order derivatives, such as an *incremental model*, thereby simplifying training. The incremental model is a local linear approximation of a nonlinear system derived using Taylor expansion. The combination with Recursive Least Squares (RLS) identification in ADP framework has led to the development of incremental model-based ADP (IADP) methods, enabling computationally efficient online policy learning. Compared with Action Dependent Heuristic Dynamic Programming (ADHDP), which implicitly approximates the control effectiveness within a state-action (Q) function, the RLS algorithm quickly and accurately identifies the local control effectiveness represented in an incremental model, leading to a more reliable construction of the policy gradient, as demonstrated in simple cases [Ref]. For example, the Incremental model-based Heuristic Dynamic Programming (IHDP) requires only the signs of control effectiveness matrix G to represent the gradient signs, representing less model information than other variants of IADP, including incremental model-based dual heuristic programming (IDHP), and incremental model-based global dual heuristic programming (IGDHP).

The theoretical analysis of online ADHDP has been studied in [Ref], where the gradient descent algorithm is used to update critic and actor over time. The weights are proved to be ultimately uniformly boundedness (UUB) to the sub-optimal weights. learning process involves three time steps. The fact is that IHDP updates the critic in the same way as ADHDP, but updates the actor using an estimated value function reconstructed according to the Bellman equation, instead of a state-action (Q) function in ADHDP. As a result, the update laws of the actor are different. In this study, we formulate the update laws of IHDP into two time steps and analyze the UUB convergence of the estimated weights considering action smoothness.

IHDP have been applied to online policy optimization for tracking control of pitch rate, angle of attack (AOA), and altitude for the Flying-V, the Cessna Citation business jet, and the F-16 fighter model.

The application of IHDP for AOA tracking control commonly uses a *cascaded* control structure to regulate angle-of-attack tracking in the outer-loop system and pitch-rate tracking in the inner-loop system, allowing a *hierarchical* control strategy that is able to explicitly incorporates pitch-rate constraints. As a comparison, the monolithic structure can also constrain the pitch rate through penalization in the reward design, but its does not learn a pitch rate reference, leading to degraded rate control performance. In addition, the rate control performance is sensitive to the weight of the pitch-rate loss term. Therefore, it is important to develop a well-designed pitch-rate reference for ensuring reliable control performance. An illustrative example is

Yifei Li was with the Section Control and Simulation, Faculty of Aerospace Engineering, Delft University of Technology, Delft, 2629 HS, the Netherlands, e-mail: y.li-34@tudelft.nl.

Erik-Jan van Kampen was with the Section Control and Simulation, Faculty of Aerospace Engineering, Delft University of Technology, Delft, 2629 HS, the Netherlands, e-mail: e.vankampen@tudelft.nl.

Manuscript received Month Day, Year; revised Month Day, Year.

backstepping, where a stabilizing pitch-rate reference policy is derived from a nominal model which ensures the convergence of tracking errors, with accompanying adaptive laws to handle model uncertainties.

However, designing a stabilizing pitch-rate reference is challenging in the model-free IHDP framework, since it relies solely on measured data for pitch-rate reference optimization, which usually leads to a destabilizing reference during learning. A challenge lies in the frequently switching tracking errors near zero caused by time-varying nonlinear dynamics and time-varying α reference signals, which is more serious than in linear time-invariant (LTI) systems. These switching tracking errors, in turn, generate switching pitch-rate references through the outer-loop actor, further perturbing the control surface deflections through the inner-loop actor. This switching phenomenon is also observed in sliding mode control systems.

A second factor contributing to state and action oscillations is actor saturation, in which case the actor uses maximum or minimum actions responding to switching near-zero tracking errors, known as bang–bang control. Meanwhile, vanishing policy gradients in the saturated regions of activation functions cause the actor weights to become nearly fixed and difficult to adjust flexibly. To mitigate this problem, discounted learning rates have been used to slow down actor updates over time, reducing the likelihood of entering the saturation region. The disadvantages lie in that discounted learning rate is selected empirically and is sensitive to its effectiveness. Also, it does not completely prevent actor saturation as learning progresses. The other solution is to terminate actor updates by fixing the weights once the required control performance is achieved, either by setting a termination time or a tracking error threshold, a strategy that has not yet been studied.

Conditioning for Action Policy Smoothness (CAPS) is an action-smoothing technique that regularizes actor smoothness in temporal and spatial scales. The first successful application is on offline-learning quadrotor control [Ref], where the temporal smoothness loss significantly reduces the amplitude of switching motor actions. Other applications are seen for Flying-V, and Cessna Citation. In this study, we only consider regularizing temporal smoothness, given the difficulty of constructing a spatial smoothness loss with limited samples in online learning. The low-pass filter has been used to remove high-frequency noise in command signals in command-filtered backstepping, Incremental Nonlinear Dynamic Inversion (INDI). The advantage of a filter is smoothing high-frequency commands by tuning the natural frequency ω_n , even the amplitude of the command is small. This compensates the disadvantage of temporal smoothness in removing low-frequency commands.

The main contributions of this study are summarized as:

- We propose temporal-smoothed IHDP method to enable smooth policy learning in online learning. The estimated weights of the critic and the actor are analyzed to converge to the sub-optimal weights in UUB sense, considering the extra policy gradients from the temporal smoothness loss.
- The temporal-smoothed IHDP is applied for cascaded online learning flight control, for angle-of-attack tracking.
- A low-pass filter is applied to reduce the switching of pitch-rate reference and control surface deflection.
- The termination and restart conditions are designed based on tracking errors over a fixed past time window, enabling adaptive online learning with flexible control of termination and restart.

The remainder of this paper is structured as follows. Section VI presents the aerial vehicle model and its formulation as a single-input–single-output system. Section ?? formulates optimization-based tracking control design. Section ?? presents the cascaded online RL framework, followed by introducing two action-smoothing techniques in Section VI-D. Section VII presents flight control simulations with action-smoothing techniques. Section VIII concludes this paper.

II. INCREMENTAL MODEL AND ONLINE IDENTIFICATION

A. Reformulation of Incremental Model

The continuous nonlinear system is given as

$$\dot{x}(t) = f(x(t), u(t)) \tag{1}$$

where the dynamics $f : \mathbb{R}^n \times \mathbb{R}^m \rightarrow \mathbb{R}^n$ is a smooth function associated with state vector $x \in \mathbb{R}^n$ and input vector $u \in \mathbb{R}^m$. n, m are positive integers denoting the dimensions of the state and action spaces.

Taking Taylor expansion for $f(x(t), u(t))$ at t_0 :

$$f(x(t), u(t)) = f(x(t_0), u(t_0)) + F(t_0)(x(t) - x(t_0)) + G(t_0)(u(t) - u(t_0)) + O \left[(x(t) - x(t_0))^2, (u(t) - u(t_0))^2 \right] \tag{2}$$

where $F(t_0) = \partial f(x, u) / \partial x|_{x(t_0), u(t_0)} \in \mathbb{R}^{n \times n}$, $G(t_0) = \partial f(x, u) / \partial u|_{x(t_0), u(t_0)} \in \mathbb{R}^{n \times m}$ are first-order partial derivatives at t_0 . $O(\cdot)$ is the summed higher-order terms.

The summed higher-order terms $O(\cdot)$ have a relatively small effect on the change from x_t to x_{t+1} compared with the first-order terms. Moreover, these higher-order derivatives are difficult to identify from data, which poses challenges for practical application of an incremental model that includes them. For these two reasons, we omit $O(\cdot)$ when defining an effective and practical model for the nonlinear system:

$$f(x(t), u(t)) = f(x(t_0), u(t_0)) + F(t_0)(x(t) - x(t_0)) + G(t_0)(u(t) - u(t_0)) \quad (3)$$

Using Equation 104:

$$\dot{x}(t) = \dot{x}(t_0) + F(t_0)[x(t) - x(t_0)] + G(t_0)[u(t) - u(t_0)] \quad (4)$$

The time derivatives are approximated by $\dot{x}(t) \approx \frac{x(t+T) - x(t)}{T}$ and $\dot{x}(t_0) \approx \frac{x(t_0+T) - x(t_0)}{T}$, where T is a constant time step. Then

$$\frac{x(t+T) - x(t)}{T} \approx \frac{x(t_0+T) - x(t_0)}{T} + F(t_0)[x(t) - x(t_0)] + G(t_0)[u(t) - u(t_0)] \quad (5)$$

Define a discretization approach over T by setting $t_0 = (k-1)T$, $x(t_0) = x((k-1)T) \triangleq x_{k-1}$. Let $x(t)$ denote the next-step state following $x(t_0)$, then $x(t) = x(t_0 + T) \triangleq x_k$.

A discretized version of system 108 is

$$x_{k+1} - x_k \approx x_k - x_{k-1} + F_{k-1}(x_k - x_{k-1})T + G_{k-1}(u_k - u_{k-1})T \quad (6)$$

Use denotions $\Delta x(k+1) = x(k+1) - x(k)$, $\Delta x(k) = x(k) - x(k-1)$, $\Delta u(k) = u(k) - u(k-1)$:

$$\Delta x_{k+1} = \Delta x_k + F_{k-1}\Delta x_k T + G_{k-1}\Delta u_k T \quad (7)$$

B. Recursive Least Squares identification

The linear forgetting Recursive Least Squares (RLS) algorithm is applied to identify matrices F_{t-1}, G_{t-1} are identified online. Define the augmented state as $\mathbf{x}_t = [\Delta q_t, \Delta \delta_t]^T$ and estimated parameter vector as $\hat{\theta}_{t-1} = [\hat{F}_{t-1}, \hat{G}_{t-1}]^T$. The one-step state prediction is made as $\Delta \hat{\mathbf{x}}_{t+1}^T = \mathbf{x}_t^T \hat{\theta}_{t-1}$. The error between the true state and the predicted state is denoted by ε_t and defined as $\varepsilon_t = \Delta \mathbf{x}_{t+1}^T - \Delta \hat{\mathbf{x}}_{t+1}^T$. The parameter matrix is updated by

$$\hat{\theta}_t = \hat{\theta}_{t-1} + P_t \mathbf{x}_t \varepsilon_t \quad (8)$$

$$\begin{aligned} P_t^{-1} &= \alpha P_{t-1}^{-1} + \mathbf{x}_t \mathbf{x}_t^T \\ &= \sum_{j=1}^t \alpha^{t-j} \mathbf{x}_j \mathbf{x}_j^T + \alpha^t P_0^{-1} \\ &= \sum_{j=1}^t \alpha^{t-j} \mathbf{x}_j \mathbf{x}_j^T + I \alpha^t \lambda_{\min}(0) \end{aligned} \quad (9)$$

The initial auxiliary matrix is set as $P_0 = I/\lambda_{\min}(0)$, where $0 < \lambda_{\min}(0) \ll 1$ is the minimum eigenvalue of P_0^{-1} . The initial parameter matrix is $\hat{\theta}_0$. The forgetting factor is $0 \ll \alpha < 1$.

III. TEMPORAL-SMOOTHED INCREMENTAL MODEL-BASED HEURISTIC DYNAMIC PROGRAMMING

A. Problem formulation

Consider a discrete-time nonlinear dynamical system as

$$x(t+1) = f(x(t), u(t)), \quad (10)$$

where $x \in \mathbb{R}^m$ is the state vector and $u \in \mathbb{R}^n$ is the control vector.

The cost-to-go function is expressed as

$$J(x(t)) = \sum_{i=t}^{\infty} \alpha^{i-t} r(x(i), u(i)), \quad (11)$$

where $\alpha \in (0, 1]$ is the discount factor, $r(x(t), u(t))$ is the reward function. We require $r(t) = r(x(t), u(t))$ to be a bounded semidefinite function of the state and control so that the cost function is well defined. One can obtain from (11) that $0 = J(t) - r(t) - \alpha J(t+1)$, where $J(t) = J(x(t))$.

B. Critic network

The critic network is a one-hidden-layer multilayer perceptron (MLP) that takes the input as $y(t) = (x_1(t), \dots, x_m(t))^T$ and the output as $\hat{J}(t)$ to approximate $J(t)$. The number of nodes in hidden layer is N_{h_c} . The weight between input node i and hidden node j is $\hat{w}_{c,ji}^{(1)}(t)$. The weight between hidden node j and output node is $\hat{w}_{c,j}^{(2)}(t)$.

The input to hidden node j is:

$$\sigma_{c,j}(t) = \sum_{i=1}^m \hat{w}_{c,ji}^{(1)}(t) x_i(t) \quad (12)$$

The output of hidden node j is

$$\phi_{c,j}(t) = \tanh(\sigma_{c,j}(t)) \quad (13)$$

where $\tanh(\cdot)$ is the nonlinear activation function.

The output of the critic is

$$\hat{J}(t) = \sum_{j=1}^{N_{h_c}} \hat{w}_{c,j}^{(2)}(t) \phi_{c,j}(t), \quad (14)$$

C. Actor network

The actor network is a one-hidden-layer multilayer perceptron (MLP) that takes the input as the state $x(t) = (x_1(t), \dots, x_m(t))^T$, and the output as the action. The number of nodes in hidden layer is N_{h_a} . The weight between input node i and hidden node j is $\hat{w}_{a,ji}^{(1)}(t)$. The weight between hidden node j and output node k is $\hat{w}_{a,kj}^{(2)}(t)$.

The input to hidden node j is

$$\sigma_{a,j}(t) = \sum_{i=1}^m \hat{w}_{a,ji}^{(1)}(t) x_i(t). \quad (15)$$

The output of hidden node j is:

$$\phi_{a,j}(t) = \tanh(\sigma_{a,j}(t)) \quad (16)$$

The output of the output node k is

$$u_k(t) = \sum_{j=1}^{N_{h_a}} \hat{w}_{a,kj}^{(2)}(t) \phi_{a,j}(t) \quad (17)$$

IV. GRADIENT-DESCENT ALGORITHM

A. Update of the critic network

The critic network is trained to minimize the objective function $E_c(t) = \frac{1}{2}e_c^2(t)$, where $e_c(t) = \hat{J}(t) - r(t) - \alpha\hat{J}(t+1)$ is the Bellman error. This definition in ADHDP [Ref] follows a backward style due to the convenience of policy improvement using state-action value function.

The weights between the input layer and the hidden layer are updated by

$$\hat{w}_c^{(1)}(t+1) = \hat{w}_c^{(1)}(t) + \Delta\hat{w}_c^{(1)}(t) \quad (18)$$

where $\hat{w}_c^{(1)} \in \mathbb{R}^{N_{h_c} \times m}$.

According to the gradient descent:

$$\Delta\hat{w}_{c,ji}^{(1)}(t) = l_c \left[-\frac{\partial E_c(t)}{\partial \hat{w}_{c,ji}^{(1)}(t)} \right] \quad (19)$$

which follows from the chain rule

$$\begin{aligned} \frac{\partial E_c(t)}{\partial \hat{w}_{c,ji}^{(1)}(t)} &= \frac{\partial E_c(t)}{\partial e_c(t)} \frac{\partial e_c(t)}{\partial \hat{J}(t)} \frac{\partial \hat{J}(t)}{\partial \phi_{c,j}(t)} \frac{\partial \phi_{c,j}(t)}{\partial \sigma_{c,j}(t)} \frac{\partial \sigma_{c,j}(t)}{\partial \hat{w}_{c,ji}^{(1)}(t)} \\ &= e_c(t) \hat{w}_{c,j}^{(2)}(t) \phi'_{c,j}(t) y_i(t) \end{aligned} \quad (20)$$

The weights between the hidden layer and the output layer are updated by

$$\hat{w}_c^{(2)}(t+1) = \hat{w}_c^{(2)}(t) + \Delta\hat{w}_c^{(2)}(t) \quad (21)$$

where $\hat{w}_c^{(2)} \in \mathbb{R}^{1 \times N_{hc}}$.

According to the gradient descent:

$$\Delta\hat{w}_{c,j}^{(2)}(t) = l_c \left[-\frac{\partial E_c(t)}{\partial \hat{w}_{c,j}^{(2)}(t)} \right] \quad (22)$$

which follows from the chain rule

$$\frac{\partial E_c(t)}{\partial \hat{w}_{c,j}^{(2)}(t)} = \frac{\partial E_c(t)}{\partial e_c(t)} \frac{\partial e_c(t)}{\partial \hat{J}(t)} \frac{\partial \hat{J}(t)}{\partial \hat{w}_{c,j}^{(2)}(t)} = e_c(t) \phi_{c,j}(t) \quad (23)$$

B. Update of the actor network

The actor network is trained according to $\hat{J}(t)$, which is reconstructed from the Bellman equation as $\hat{J}(t) = r(t) + \alpha\hat{J}(t+1)$, rather than a state-action value function $\hat{J}(x(t), u(t))$ as in ADHDP [Ref]. (In this paper, we use an importance-weighted training approach). (Let U_c denote the desired ultimate objective function. The quadratic error measure to be minimized is $E_a(t) = E_a^1(t) + E_a^2(t)$, $E_a^1(t) = \frac{1}{2}e_a^2(t)$, $E_a^2(t) = \frac{1}{2}\lambda e_s^2(t)$, $e_a(t) = r(t) + \alpha\hat{J}(t+1) - U_c$, $e_s(t) = \frac{1}{2}\|u(t) - u(t+1)\|^2$. $e_s(t)$ is a temporal smoothness measure. In reinforcement learning, success corresponds to an objective that is zero at each time step. For simplicity of derivation, we assume $U_c = 0$, i.e. $e_a(t) = r(t) + \alpha\hat{J}(t+1)$).

The gradient-descent update rule is $\hat{w}_a(t+1) = \hat{w}_a(t) + \Delta\hat{w}_a(t)$, where $\Delta\hat{w}_a(t) = l_a \left[-\frac{\partial E_a(t)}{\partial \hat{w}_a(t)} \right]$, $l_a > 0$.

The weights between the input layer and the hidden layer is updated by

$$\hat{w}_a^{(1)}(t+1) = \hat{w}_a^{(1)}(t) + \Delta\hat{w}_a^{(1)}(t) \quad (24)$$

where $\hat{w}_a^{(1)} \in \mathbb{R}^{N_{hc} \times m}$, and the element-wise increment:

$$\Delta\hat{w}_{a,ji}^{(1)}(t) = l_a \left[-\frac{\partial E_a^1(t)}{\partial \hat{w}_{a,ji}^{(1)}(t)} - \frac{\partial E_a^2(t)}{\partial \hat{w}_{a,ji}^{(1)}(t)} \right], \quad (25)$$

Applying the chain rule:

$$\begin{aligned} \frac{\partial E_a^1(t)}{\partial \hat{w}_{a,ji}^{(1)}(t)} &= \frac{\partial E_a^1(t)}{\partial e_a(t)} \left[\frac{\partial e_a(t)}{\partial u(t)} \right]^T \frac{\partial u(t)}{\partial \phi_{a,j}(t)} \frac{\partial \phi_{a,j}(t)}{\partial \sigma_{a,j}(t)} \frac{\partial \sigma_{a,j}(t)}{\partial \hat{w}_{a,ji}^{(1)}(t)} \\ &= \frac{\partial E_a^1(t)}{\partial e_a(t)} \sum_{k=1}^n \frac{\partial e_a(t)}{\partial u_k(t)} \frac{\partial u_k(t)}{\partial \phi_{a,j}(t)} \frac{\partial \phi_{a,j}(t)}{\partial \sigma_{a,j}(t)} \frac{\partial \sigma_{a,j}(t)}{\partial \hat{w}_{a,ji}^{(1)}(t)} \\ &= \frac{\partial E_a^1(t)}{\partial e_a(t)} \sum_{k=1}^n \left(\frac{\partial r(t)}{\partial u(t)} + \alpha \left[\frac{\partial \hat{J}(t+1)}{\partial x(t+1)} \right]^T \frac{\partial x(t+1)}{\partial u(t)} \right)_k \frac{\partial u_k(t)}{\partial \phi_{a,j}(t)} \frac{\partial \phi_{a,j}(t)}{\partial \sigma_{a,j}(t)} \frac{\partial \sigma_{a,j}(t)}{\partial \hat{w}_{a,ji}^{(1)}(t)} \\ &= \frac{\partial E_a^1(t)}{\partial e_a(t)} \sum_{k=1}^n \left(2Ru(t) + \alpha \left[\frac{\partial \hat{J}(t+1)}{\partial x(t+1)} \right]^T G(t-1) \right)_k \frac{\partial u_k(t)}{\partial \phi_{a,j}(t)} \frac{\partial \phi_{a,j}(t)}{\partial \sigma_{a,j}(t)} \frac{\partial \sigma_{a,j}(t)}{\partial \hat{w}_{a,ji}^{(1)}(t)} \\ &= e_a(t) \sum_{k=1}^n \left(2Ru(t) + \left[\alpha\hat{w}_c^{(2)}(t)\phi'(x(t+1))\hat{w}_c^{(1)}(t) \right]^T G(t-1) \right)_k \hat{w}_{a,kj}^{(2)}(t)\phi'_{a,j}(x(t))x_i(t) \end{aligned} \quad (26)$$

and

$$\begin{aligned} \frac{\partial E_a^2(t)}{\partial \hat{w}_{a,ji}^{(1)}(t)} &= \frac{\partial E_a^2(t)}{\partial e_s(t)} \left[\frac{\partial e_s(t)}{\partial u(t)} \right]^T \frac{\partial u(t)}{\partial \phi_{a,j}(t)} \frac{\partial \phi_{a,j}(t)}{\partial \sigma_{a,j}(t)} \frac{\partial \sigma_{a,j}(t)}{\partial \hat{w}_{a,ji}^{(1)}(t)} \\ &= \frac{\partial E_a^2(t)}{\partial e_s(t)} \sum_{k=1}^n \frac{\partial e_s(t)}{\partial u_k(t)} \frac{\partial u_k(t)}{\partial \phi_{a,j}(t)} \frac{\partial \phi_{a,j}(t)}{\partial \sigma_{a,j}(t)} \frac{\partial \sigma_{a,j}(t)}{\partial \hat{w}_{a,ji}^{(1)}(t)} \\ &= e_s(t) \sum_{k=1}^n (u_k(t) - u_k(t+1))\hat{w}_{a,kj}^{(2)}(t)\phi'_{a,j}(x(t))x_i(t) \end{aligned} \quad (27)$$

The weight between the hidden layer and the output layer is updated by

$$\hat{w}_a^{(2)}(t+1) = \hat{w}_a^{(2)}(t) + \Delta \hat{w}_a^{(2)}(t) \quad (28)$$

where $\hat{w}_a^{(2)} \in \mathbb{R}^{n \times N_{h_a}}$, and the element-wise increment:

$$\Delta \hat{w}_{a,kj}^{(2)}(t) = l_a \left[-\frac{\partial E_a^1(t)}{\partial \hat{w}_{a,kj}^{(2)}(t)} - \frac{\partial E_a^2(t)}{\partial \hat{w}_{a,kj}^{(2)}(t)} \right] \quad (29)$$

Applying the chain rule:

$$\begin{aligned} \frac{\partial E_a^1(t)}{\partial \hat{w}_{a,kj}^{(2)}(t)} &= \frac{\partial E_a^1(t)}{\partial e_a(t)} \frac{\partial e_a(t)}{\partial u_k(t)} \frac{\partial u_k(t)}{\partial \hat{w}_{a,kj}^{(2)}(t)} \\ &= \frac{\partial E_a^1(t)}{\partial e_a(t)} \left(\frac{\partial r(t)}{\partial u(t)} + \alpha \left[\frac{\partial \hat{J}(t+1)}{\partial x(t+1)} \right]^T \frac{\partial x(t+1)}{\partial u(t)} \right)_k \frac{\partial u_k(t)}{\partial \hat{w}_{a,kj}^{(2)}(t)} \\ &= e_a(t) \left(2Ru(t) + \alpha \left[\frac{\partial \hat{J}(t+1)}{\partial x(t+1)} \right]^T G(t-1) \right)_k \phi_{a,j}(t) \\ &= e_a(t) \left(2Ru(t) + \left[\alpha \hat{w}_c^{(2)}(t) \phi'(x(t+1)) \hat{w}_c^{(1)}(t) \right]^T G(t-1) \right)_k \phi_{a,j}(t) \end{aligned} \quad (30)$$

and

$$\begin{aligned} \frac{\partial E_a^2(t)}{\partial \hat{w}_{a,kj}^{(2)}(t)} &= \frac{\partial E_a^2(t)}{\partial e_s(t)} \frac{\partial e_s(t)}{\partial u_k(t)} \frac{\partial u_k(t)}{\partial \hat{w}_{a,kj}^{(2)}(t)} \\ &= e_s(t) (u_k(t) - u_k(t+1)) \phi_{a,j}(t) \end{aligned} \quad (31)$$

Remark 1. The essence of IHDP is abstracting the control effectiveness matrix of the dynamical system $G(t-1)$ from a state-action function in Action Dependent Heuristic Dynamic Programming (ADHDP) framework, to improve the learning accuracy and efficiency. The matrix G is identified using Recursive Least Square (RLS) algorithm online.

V. CONVERGENCE ANALYSIS

A. Basics of uniformly ultimately bounded stability

Denote the sub-optimal weights by w_c^* , w_a^* , defined as $w_c^* = \arg \min_{\hat{w}_c} \left\| \hat{J}(t) - r(t) - \alpha \hat{J}(t+1) \right\|$, and $w_a^* = \arg \min_{\hat{w}_a} \left\| r(t) + \alpha \hat{J}(t+1) - U_c \right\|$ if assuming $U_c = 0$. The estimation errors of the critic and actor weights are defined by $\tilde{w}(t) := \hat{w}(t) - w^*$. Then Equations 20, 23, 26,31 define a dynamical system of estimation errors for a nonlinear function F :

$$\tilde{w}(t+1) = \tilde{w}(t) - F(\hat{w}(t), \phi(t), \phi(t+1)) \quad (32)$$

Definition 1. A dynamical system is said to be uniformly ultimately bounded (UUB) with ultimate bound $b > 0$, if for any $a > 0$ and $t_0 > 0$, there exists a positive number $N = N(a, b)$ independent of t_0 , such that $\|\tilde{w}(t)\| \leq b$, for all $t \geq N + t_0$, whenever $\|\tilde{w}(t_0)\| \leq a$.

Theorem 1 (UUB of a discrete dynamical system). If, for system (32), there exists a function $L(\tilde{w}(t), t)$ such that for all $\tilde{w}(t_0)$ in a compact set K , $L(\tilde{w}(t), t)$ is positive definite and the first difference satisfies $\Delta L(\tilde{w}(t), t) < 0$, for $\|\tilde{w}(t_0)\| > b$, for some $b > 0$ such that the b -neighborhood of $\tilde{w}(t)$ is contained in K , then the system is UUB and the norm of the state is bounded within a neighborhood of b .

B. Network weights increments

The convergence of critic and actor weights is analyzed using gradient descent algorithm. The requirements on learning rate to stabilize the convergence are analyzed. The ultimate bound is also provided.

Assumption 1. The sub-optimal weights are bounded as $\|w_c^*\| \leq w_c^{\max}$, $\|w_a^*\| \leq w_a^{\max}$.

Lemma 1. Under Assumption 1, define $L_1(t) = \frac{1}{l_c} \text{tr} \left[(\tilde{w}_c^{(2)}(t))^T \tilde{w}_c^{(2)}(t) \right]$, and its first difference $\Delta L_1(t) = L_1(t+1) - L_1(t)$ is

$$\Delta L_1(t) = l_c e_c^2(t) \|\phi_c(t)\|^2 + \|e_c(t) - \tilde{w}_c^{(2)}(t) \phi_c(t)\|^2 - \|\zeta_c(t)\|^2 - e_c^2(t) \quad (33)$$

where $\zeta_c(t) = \tilde{w}_c^{(2)}(t) \phi_c(t)$ is the approximation error of the critic output.

Proof. According to (21), (22), (23) and the fact that $w_c^{*(2)}$ is time-invariant:

$$\tilde{w}_c^{(2)}(t+1) = \hat{w}_c^{(2)}(t+1) - w_c^{*(2)} = \tilde{w}_c^{(2)}(t) - l_c e_c(t) \phi_c^T(t) \quad (34)$$

where $\phi_c(t) \in \mathbb{R}^{N_{h_c} \times 1}$, $e_c(t)$ is a scalar. The quadratic weight error is

$$\begin{aligned} \text{tr} \left[\left(\tilde{w}_c^{(2)}(t+1) \right)^T \tilde{w}_c^{(2)}(t+1) \right] &= \text{tr} \left[\left(\tilde{w}_c^{(2)}(t) - l_c e_c(t) \phi_c^T(t) \right)^T \left(\tilde{w}_c^{(2)}(t) - l_c e_c(t) \phi_c^T(t) \right) \right] \\ &= \text{tr} \left[\left(\hat{w}_c^{(2)}(t) \right)^T \tilde{w}_c^{(2)}(t) \right] + \text{tr} \left[l_c^2 e_c^2(t) \phi_c(t) \phi_c^T(t) \right] \\ &\quad - l_c e_c(t) \text{tr} \left[\left(\tilde{w}_c^{(2)}(t) \right)^T \phi_c^T(t) \right] - l_c e_c(t) \text{tr} \left[\phi_c(t) \tilde{w}_c^{(2)}(t) \right] \\ &= \text{tr} \left[\left(\hat{w}_c^{(2)}(t) \right)^T \tilde{w}_c^{(2)}(t) \right] + \text{tr} \left[l_c^2 e_c^2(t) \phi_c(t) \phi_c^T(t) \right] \\ &\quad - 2l_c e_c(t) \text{tr} \left[\phi_c(t) \tilde{w}_c^{(2)}(t) \right] \\ &= \text{tr} \left[\left(\hat{w}_c^{(2)}(t) \right)^T \tilde{w}_c^{(2)}(t) \right] + l_c^2 e_c^2(t) \|\phi_c(t)\|^2 \\ &\quad - 2l_c e_c(t) \tilde{w}_c^{(2)}(t) \phi_c(t) \end{aligned} \quad (35)$$

Since $\tilde{w}_c^{(2)}(t) \phi_c(t)$ is a scalar, the cross term becomes

$$-2l_c e_c(t) \tilde{w}_c^{(2)}(t) \phi_c(t) = l_c \left(\|e_c(t) - \tilde{w}_c^{(2)}(t) \phi_c(t)\|^2 - \|\tilde{w}_c^{(2)}(t) \phi_c(t)\|^2 - e_c^2(t) \right) \quad (36)$$

The difference $\Delta L_1(t)$ yields

$$\begin{aligned} \Delta L_1(t) &= \frac{1}{l_c} \left(\text{tr} \left[\left(\tilde{w}_c^{(2)}(t+1) \right)^T \tilde{w}_c^{(2)}(t+1) \right] - \text{tr} \left[\left(\tilde{w}_c^{(2)}(t) \right)^T \tilde{w}_c^{(2)}(t) \right] \right) \\ &= l_c e_c^2(t) \|\phi_c(t)\|^2 + \|e_c(t) - \tilde{w}_c^{(2)}(t) \phi_c(t)\|^2 - \|\tilde{w}_c^{(2)}(t) \phi_c(t)\|^2 - e_c^2(t) \\ &= \underbrace{l_c e_c^2(t) \|\phi_c(t)\|^2 + \|e_c(t) - \tilde{w}_c^{(2)}(t) \phi_c(t)\|^2 - \|\zeta_c(t)\|^2 - e_c^2(t)}_{\Delta L_1(t)} \end{aligned} \quad (37)$$

where $\zeta_c(t) = \tilde{w}_c^{(2)}(t) \phi_c(t)$. □

Lemma 2. Under Assumption 1, define $L_2(t) = \frac{1}{l_a \gamma_1} \text{tr} \left[\left(\tilde{w}_a^{(2)}(t) \right)^T \tilde{w}_a^{(2)}(t) \right]$, and its first difference $\Delta L_2(t) = L_2(t+1) - L_2(t)$ is bounded by

$$\Delta L_2(t) \leq \frac{1}{\gamma_1} \left(l_a e_a^2(t) \|C(t)\|^2 \|\phi_a(t)\|^2 + 4\|r(t)\|^2 + 8\alpha^2 \|\zeta_c(t+1)\|^2 + 8\alpha^2 \left\| w_c^{*(2)} \phi_c(t+1) \right\|^2 + \|C(t)\|^2 \|\zeta_a(t)\|^2 - e_a^2(t) \right) \quad (38)$$

where $\zeta_a(t) = \tilde{w}_a^{(2)}(t) \phi_a(t)$.

Proof. According to (28), (29), (31) and the fact that $w_a^{*(2)}$ is time-invariant:

$$\tilde{w}_a^{(2)}(t+1) = \hat{w}_a^{(2)}(t+1) - w_a^{*(2)} = \tilde{w}_a^{(2)}(t) - l_a e_a(t) C(t) \phi_a^T(t) \quad (39)$$

where $\phi_a \in \mathbb{R}^{N_{a_n} \times 1}$, $C(t) \in \mathbb{R}^{n \times 1}$ and its element $C_k(t) = \left(2Ru(t) + \left[\alpha \hat{w}_c^{(2)}(t) \phi'(x(t+1)) \hat{w}_c^{(1)}(t) \right]^T G(t-1) \right)_k$.

The trace of the quadratic weight error is

$$\begin{aligned}
 \text{tr} \left[\left(\tilde{w}_a^{(2)}(t+1) \right)^T \tilde{w}_a^{(2)}(t+1) \right] &= \text{tr} \left[\left(\tilde{w}_a^{(2)}(t) - l_a e_a(t) C(t) \phi_a^T(t) \right)^T \left(\tilde{w}_a^{(2)}(t) - l_a e_a(t) C(t) \phi_a^T(t) \right) \right] \\
 &= \text{tr} \left[\left(\tilde{w}_a^{(2)}(t) \right)^T \tilde{w}_a^{(2)}(t) \right] + \text{tr} \left[l_a^2 e_a^2(t) \phi_a(t) C^T(t) C(t) \phi_a^T(t) \right] \\
 &\quad - l_a e_a(t) \text{tr} \left[\left(\tilde{w}_a^{(2)}(t) \right)^T C(t) \phi_a^T(t) \right] - l_a e_a(t) \text{tr} \left[\phi_a(t) C^T(t) \tilde{w}_a^{(2)}(t) \right] \\
 &= \text{tr} \left[\left(\tilde{w}_a^{(2)}(t) \right)^T \tilde{w}_a^{(2)}(t) \right] + \text{tr} \left[l_a^2 e_a^2(t) \phi_a(t) C^T(t) C(t) \phi_a^T(t) \right] \\
 &\quad - 2l_a e_a(t) \text{tr} \left[\phi_a(t) C^T(t) \tilde{w}_a^{(2)}(t) \right]
 \end{aligned} \tag{40}$$

Consider the cross term, and use $\text{tr}(ABC) = \text{tr}(CAB)$:

$$\begin{aligned}
 -2l_a e_a(t) \text{tr} \left(\phi_a(t) C^T(t) \tilde{w}_a^{(2)}(t) \right) &= -2l_a e_a(t) \text{tr} \left(C^T(t) \tilde{w}_a^{(2)}(t) \phi_a(t) \right) \\
 &= -2l_a e_a(t) C^T(t) \tilde{w}_a^{(2)}(t) \phi_a(t) \\
 &\leq l_a \left(\left\| e_a(t) - C^T(t) \tilde{w}_a^{(2)}(t) \phi_a(t) \right\|^2 - \left\| C^T(t) \tilde{w}_a^{(2)}(t) \phi_a(t) \right\|^2 - e_a^2(t) \right) \\
 &\leq l_a \left(\left\| e_a(t) - C^T(t) \zeta_a(t) \right\|^2 - \left\| C^T(t) \zeta_a(t) \right\|^2 - e_a^2(t) \right)
 \end{aligned} \tag{41}$$

where $\zeta_a(t) = \tilde{w}_a^{(2)}(t) \phi_a(t)$.

Notice that $(a-b)^2 - b^2 \leq 2a^2 + b^2$, and use $\|C^T(t)\zeta_a(t)\|^2 \leq \|C^T(t)\|^2 \|\zeta_a(t)\|^2$ by Cauchy–Schwarz inequality:

$$\begin{aligned}
 &\left\| e_a(t) - C^T(t) \zeta_a(t) \right\|^2 - \left\| C^T(t) \zeta_a(t) \right\|^2 \\
 &\leq 2 \left\| e_a(t) \right\|^2 + \left\| C^T(t) \zeta_a(t) \right\|^2 \\
 &\leq 2 \left\| r(t) + \alpha \hat{J}(t+1) \right\|^2 + \left\| C^T(t) \zeta_a(t) \right\|^2 \\
 &\leq 2 \left(\left\| r(t) \right\| + \alpha \left\| \hat{J}(t+1) \right\| \right)^2 + \left\| C^T(t) \zeta_a(t) \right\|^2 \\
 &\leq 4 \left\| r(t) \right\|^2 + 4\alpha^2 \left\| \hat{w}_c^{(2)} \phi_c(t+1) \right\|^2 + \left\| C^T(t) \zeta_a(t) \right\|^2 \\
 &\leq 4 \left\| r(t) \right\|^2 + 4\alpha^2 \left\| (\tilde{w}_c^{(2)} + w_c^{*(2)}) \phi_c(t+1) \right\|^2 + \left\| C^T(t) \zeta_a(t) \right\|^2 \\
 &\leq 4 \left\| r(t) \right\|^2 + 8\alpha^2 \left\| \tilde{w}_c^{(2)} \phi_c(t+1) \right\|^2 + 8\alpha^2 \left\| w_c^{*(2)} \phi_c(t+1) \right\|^2 + \left\| C^T(t) \zeta_a(t) \right\|^2 \\
 &\leq 4 \left\| r(t) \right\|^2 + 8\alpha^2 \left\| \zeta_c(t+1) \right\|^2 + 8\alpha^2 \left\| w_c^{*(2)} \phi_c(t+1) \right\|^2 + \left\| C^T(t) \zeta_a(t) \right\|^2 \\
 &\leq 4 \left\| r(t) \right\|^2 + 8\alpha^2 \left\| \zeta_c(t+1) \right\|^2 + 8\alpha^2 \left\| w_c^{*(2)} \phi_c(t+1) \right\|^2 + \|C(t)\|^2 \|\zeta_a(t)\|^2
 \end{aligned} \tag{42}$$

where $\zeta_c(t+1) = \tilde{w}_c^{(2)} \phi_c(t+1)$.

Therefore, the first difference is

$$\begin{aligned}
 \Delta L_2(t) &= \frac{1}{l_a \gamma_1} \text{tr} \left(\tilde{w}_a^{(2)}(t+1)^T \tilde{w}_a^{(2)}(t+1) - \tilde{w}_a^{(2)}(t)^T \tilde{w}_a^{(2)}(t) \right) \\
 &\leq \frac{1}{\gamma_1} \left(l_a e_a^2(t) \|C(t)\|^2 \|\phi_a(t)\|^2 + 4 \left\| r(t) \right\|^2 + 8\alpha^2 \left\| \zeta_c(t+1) \right\|^2 + 8\alpha^2 \left\| w_c^{*(2)} \phi_c(t+1) \right\|^2 + \|C(t)\|^2 \|\zeta_a(t)\|^2 - e_a^2(t) \right)
 \end{aligned} \tag{43}$$

□

Remark 2. Note that ΔL_2 depends on $C(t)$, which incorporates the control-effectiveness matrix G_{t-1} . Thus, a system with high control effectiveness, i.e. a more “sensitive” system, may exhibit a larger bound. Intuitively, this matches our expectation.

Remark 3. $C(t)$ is defined differently from [Ref] given the objective function to improve the policy, i.e., $r(t) + \hat{J}(t+1)$ in IHDP and $\hat{J}(t)$ in ADHDP.

Remark 4. If we introduce the normalization $\|(\hat{w}_c^{(2)}(t))^T C(t)\|^2 = 1$ and fix the input-layer weights, then Lemmas 1–2 yield the results of Liu et al. (2012).

Lemma 3. Under Assumption 1, define $L_3(t) = \frac{1}{l_c \gamma_2} \text{tr} \left[(\tilde{w}_c^{(1)}(t))^T \tilde{w}_c^{(1)}(t) \right]$, and its difference $\Delta L_3(t) = L_3(t+1) - L_3(t)$ is bounded by

$$\Delta L_3(t) \leq \frac{1}{\gamma_2} \left(l_c e_c^2(t) \|a(t)\|^2 \|y(t)\|^2 + \|a(t)\|^2 \|\tilde{w}_c^{(1)}(t) y(t)\|^2 + e_c^2(t) \right) \quad (44)$$

where $\gamma_2 > 0$ is a weighting factor and $a(t) \in \mathbb{R}^{N_{h_c} \times 1}$ is a vector with $a_j(t) = \hat{w}_{c,j}^{(2)}(t) \phi_j'(t)$.

Proof. Consider the update rule (20), the weight error is

$$\tilde{w}_c^{(1)}(t+1) = \hat{w}_c^{(1)}(t+1) - w_c^{*(1)} = \tilde{w}_c^{(1)}(t) - l_c e_c(t) B(t) \quad (45)$$

where $B(t) \in \mathbb{R}^{N_{h_c} \times m}$ and its element $B_{ji}(t) = \hat{w}_{c,j}^{(2)}(t) \phi_j'(t) y_i(t)$, then $B(t) = a(t) y^T(t)$.

The quadratic weight error is

$$\begin{aligned} \text{tr} \left[\tilde{w}_c^{(1)}(t+1)^T \tilde{w}_c^{(1)}(t+1) \right] &= \text{tr} \left[\left(\tilde{w}_c^{(1)}(t) - l_c e_c(t) B(t) \right)^T \left(\tilde{w}_c^{(1)}(t) - l_c e_c(t) B(t) \right) \right] \\ &= \text{tr} \left[(\tilde{w}_c^{(1)}(t))^T \tilde{w}_c^{(1)}(t) \right] + \text{tr} \left[l_c^2 e_c^2(t) B^T(t) B(t) \right] \\ &\quad - l_c e_c(t) \left[(\tilde{w}_c^{(1)}(t))^T B(t) \right] - l_c e_c(t) \text{tr} \left[B^T(t) \tilde{w}_c^{(1)}(t) \right] \\ &= \text{tr} \left[(\tilde{w}_c^{(1)}(t))^T \tilde{w}_c^{(1)}(t) \right] + \text{tr} \left[l_c^2 e_c^2(t) B^T(t) B(t) \right] \\ &\quad - 2l_c e_c(t) \text{tr} \left[B^T(t) \tilde{w}_c^{(1)}(t) \right] \\ &= \text{tr} \left[(\tilde{w}_c^{(1)}(t))^T \tilde{w}_c^{(1)}(t) \right] + \text{tr} \left[l_c^2 e_c^2(t) y(t) a^T(t) a(t) y^T(t) \right] \\ &\quad - 2l_c e_c(t) \text{tr} \left[B^T(t) \tilde{w}_c^{(1)}(t) \right] \\ &= \text{tr} \left[(\tilde{w}_c^{(1)}(t))^T \tilde{w}_c^{(1)}(t) \right] + l_c^2 e_c^2(t) \|a(t)\|^2 \|y(t)\|^2 \\ &\quad - 2l_c e_c(t) \text{tr} \left[B^T(t) \tilde{w}_c^{(1)}(t) \right] \end{aligned} \quad (46)$$

where by $\text{tr}(ABC) = \text{tr}(BCA)$:

$$\begin{aligned} \text{tr} \left[B^T(t) \tilde{w}_c^{(1)}(t) \right] &= \text{tr} \left[y(t) a^T(t) \tilde{w}_c^{(1)}(t) \right] \\ &= \text{tr} \left[a^T(t) \tilde{w}_c^{(1)}(t) y(t) \right] \\ &= a^T(t) \tilde{w}_c^{(1)}(t) y(t) \end{aligned} \quad (47)$$

Use inequality $-2ab \leq a^2 + b^2$, the cross term becomes

$$\begin{aligned} -2l_c e_c(t) a^T(t) \tilde{w}_c^{(1)}(t) y(t) &\leq l_c \left(\|a^T(t) \tilde{w}_c^{(1)}(t) y(t)\|^2 + e_c^2(t) \right) \\ &\leq l_c \left(\|a^T(t)\|^2 \|\tilde{w}_c^{(1)}(t) y(t)\|^2 + e_c^2(t) \right) \\ &\leq l_c \left(\|a(t)\|^2 \|\tilde{w}_c^{(1)}(t) y(t)\|^2 + e_c^2(t) \right) \end{aligned} \quad (48)$$

Therefore, the first difference can be bounded by

$$\Delta L_3(t) \leq \underbrace{\frac{1}{\gamma_2} \left(l_c e_c^2(t) \|a(t)\|^2 \|y(t)\|^2 + \|a(t)\|^2 \|\tilde{w}_c^{(1)}(t) y(t)\|^2 + e_c^2(t) \right)}_{\Delta L_3(t)} \quad (49)$$

□

Lemma 4. Under Assumption 1, define $L_4(t) = \frac{1}{l_a \gamma_3} \text{tr} \left[\tilde{w}_a^{(1)}(t)^T \tilde{w}_a^{(1)}(t) \right]$, and its first difference is bounded by

$$\Delta L_4(t) \leq \frac{1}{\gamma_3} \left(l_a e_a^2(t) \|C^T(t) D(t)\|^2 \|x(t)\|^2 + e_a^2(t) + \|C^T(t) D(t)\|^2 \left\| \tilde{w}_a^{(1)}(t) x(t) \right\|^2 \right) \quad (50)$$

where $\gamma_3 > 0$ is a weighting factor, and $D(t) \in \mathbb{R}^{2 \times N_{h_a}}$, and its element $D_{kj}(t) = \hat{w}_{a,kj}^{(2)}(t) \sigma_j'(x(t))$.

Proof. According to (26), the weight errors are

$$\begin{aligned}\tilde{w}_a^{(1)}(t+1) &= \hat{w}_a^{(1)}(t+1) - w_a^{*(1)} \\ &= \tilde{w}_a^{(1)}(t) - l_a e_a(t) D^T(t) C(t) x^T(t)\end{aligned}\quad (51)$$

and

$$\begin{aligned}\text{tr} \left[\left(\tilde{w}_a^{(1)}(t+1) \right)^T \tilde{w}_a^{(1)}(t+1) \right] &= \text{tr} \left[\left(\tilde{w}_a^{(1)}(t) - l_a e_a(t) D^T(t) C(t) x^T(t) \right)^T \left(\tilde{w}_a^{(1)}(t) - l_a e_a(t) D^T(t) C(t) x^T(t) \right) \right] \\ &= \text{tr} \left[\left(\tilde{w}_a^{(1)}(t) \right)^T \tilde{w}_a^{(1)}(t) \right] + \text{tr} \left[l_a^2 e_a^2(t) x(t) C^T(t) D(t) D^T(t) C(t) x^T(t) \right] \\ &\quad - l_a e_a(t) \text{tr} \left[\left(\tilde{w}_a^{(1)}(t) \right)^T D^T(t) C(t) x^T(t) \right] - l_a e_a(t) \text{tr} \left[x(t) C^T(t) D(t) \tilde{w}_a^{(1)}(t) \right] \\ &= \text{tr} \left[\left(\tilde{w}_a^{(1)}(t) \right)^T \tilde{w}_a^{(1)}(t) \right] + l_a^2 e_a^2(t) \text{tr} \left[x(t) C^T(t) D(t) D^T(t) C(t) x^T(t) \right] \\ &\quad - 2l_a e_a(t) \text{tr} \left[x(t) C^T(t) D(t) \tilde{w}_a^{(1)}(t) \right] \\ &= \text{tr} \left[\left(\tilde{w}_a^{(1)}(t) \right)^T \tilde{w}_a^{(1)}(t) \right] + l_a^2 e_a^2(t) \|C^T(t) D(t)\|^2 \|x(t)\|^2 \\ &\quad - 2l_a e_a(t) \text{tr} \left[x(t) C^T(t) D(t) \tilde{w}_a^{(1)}(t) \right]\end{aligned}\quad (52)$$

Use $\text{tr}(ABC) = \text{tr}(BCA)$ and the fact that $C^T(t)D(t)\tilde{w}_a^{(1)}(t)x(t)$ is a scalar:

$$\begin{aligned}\text{tr} \left[x(t) C^T(t) D(t) \tilde{w}_a^{(1)}(t) \right] &= \text{tr} \left[C^T(t) D(t) \tilde{w}_a^{(1)}(t) x(t) \right] \\ &= C^T(t) D(t) \tilde{w}_a^{(1)}(t) x(t)\end{aligned}\quad (53)$$

The cross term can be transformed into the form using $-2ab \leq a^2 + b^2$ and Cauchy–Schwarz inequality:

$$\begin{aligned}-2l_a e_a(t) C^T(t) D(t) \tilde{w}_a^{(1)}(t) x(t) &\leq l_a \left(e_a^2(t) + \left\| C^T(t) D(t) \tilde{w}_a^{(1)}(t) x(t) \right\|^2 \right) \\ &\leq l_a \left(e_a^2(t) + \|C^T(t) D(t)\|^2 \|\tilde{w}_a^{(1)}(t) x(t)\|^2 \right)\end{aligned}\quad (54)$$

Finally, we can obtain the upper bound

$$\Delta L_4(t) \leq \underbrace{\frac{1}{\gamma_3} \left(l_a e_a^2(t) \|C^T(t) D(t)\|^2 \|x(t)\|^2 + e_a^2(t) + \|C^T(t) D(t)\|^2 \left\| \tilde{w}_a^{(1)}(t) x(t) \right\|^2 \right)}_{\Delta L_4(t)}\quad (55)$$

□

C. Convergence of the weights errors

We introduce the Lyapunov candidate

$$L(t) = L_1(t) + L_2(t) + L_3(t) + L_4(t)\quad (56)$$

Theorem 2 (Main Theorem). Let the weights of the critic and actor be updated by gradient descent algorithm, and assume that the reward signal is a bounded semidefinite function. Under Assumption 1, the estimation errors $w_a^* - \hat{w}_a(t)$ and $w_c^* - \hat{w}_c(t)$ are uniformly ultimately bounded (UUB) if

$$l_c < \min_t \frac{\gamma_2 - 1}{\gamma_2 (\|\phi_c(t)\|^2 + \frac{1}{\gamma_2} \|a(t)\|^2 \|y(t)\|^2)}\quad (57)$$

$$l_a < \min_t \frac{\gamma_3 - \gamma_1}{\gamma_3 \|C(t)\|^2 \|\phi_a(t)\|^2 + \gamma_1 \|D(t) C^T\|^2 \|x(t)\|^2}\quad (58)$$

Proof of Theorem 2. Collect all terms of $\Delta L(t)$ based on the results of Lemmas 1–4, $\Delta L(t)$ is bounded by

$$\Delta L(t) \leq (\Delta L_1) = l_c \underbrace{e_c^2(t)}_2 \|\phi_c(t)\|^2 + \|e_c(t) - \tilde{w}_c^{(2)}(t)\phi_c(t)\|^2 - \underbrace{\|\zeta_c(t)\|^2}_1 - \underbrace{e_c^2(t)}_2 \quad (59)$$

$$(\Delta L_2) + \frac{1}{\gamma_1} \left(l_a \underbrace{e_a^2(t)}_3 \|C(t)\|^2 \|\phi_a(t)\|^2 + 4\|r(t)\|^2 + 8\alpha^2 \underbrace{\|\zeta_c(t+1)\|^2}_1 + 8\alpha^2 \left\| w_c^{*(2)}\phi_c(t+1) \right\|^2 + \|C(t)\|^2 \|\zeta_a(t)\|^2 - \underbrace{e_a^2(t)}_3 \right) \quad (60)$$

$$(\Delta L_3) + \frac{1}{\gamma_2} \left(l_c \underbrace{e_c^2(t)}_2 \|a(t)\|^2 \|y(t)\|^2 + \|a(t)\|^2 \|\tilde{w}_c^{(1)}(t)y(t)\|^2 + \underbrace{e_c^2(t)}_2 \right) \quad (61)$$

$$\Delta L_4(t) + \frac{1}{\gamma_3} \left(l_a \underbrace{e_a^2(t)}_3 \|C^T(t)D(t)\|^2 \|x(t)\|^2 + \underbrace{e_a^2(t)}_3 + \|C^T(t)D(t)\|^2 \left\| \tilde{w}_a^{(1)}(t)x(t) \right\|^2 \right) \quad (62)$$

After combining like terms, the expression simplifies to

$$\begin{aligned} \Delta L(t) \leq & - \underbrace{\left(\|\zeta_c(t)\|^2 - \frac{8\alpha^2}{\gamma_1} \|\zeta_c(t+1)\|^2 \right)}_1 - \underbrace{\left(1 - l_c \|\phi_c(t)\|^2 - \frac{l_c}{\gamma_2} \|a(t)\|^2 \|y(t)\|^2 - \frac{1}{\gamma_2} \right) e_c^2(t)}_2 \\ & - \underbrace{\left(\frac{1}{\gamma_1} - \frac{l_a}{\gamma_1} \|C(t)\|^2 \|\phi_a(t)\|^2 - \frac{l_a}{\gamma_3} \|D(t)C^T(t)\|^2 \|x(t)\|^2 - \frac{1}{\gamma_3} \right) e_a^2(t)}_3 \\ & + \|w_c^{*(2)}(t)\phi_c(t) - r(t) - \alpha \hat{w}_c^{(2)}(t)\phi_c(t+1)\|^2 + 4\|r(t)\|^2 + \frac{8\alpha^2}{\gamma_1} \|w_c^{*(2)}\phi_c(t+1)\|^2 + \frac{1}{\gamma_1} \|C(t)\|^2 \|\zeta_a(t)\|^2 \\ & + \frac{1}{\gamma_2} \|a(t)\|^2 \|\tilde{w}_c^{(1)}(t)y(t)\|^2 \\ & + \frac{1}{\gamma_3} \|C^T(t)D(t)\|^2 \|\tilde{w}_a^{(1)}(t)x(t)\|^2 \end{aligned} \quad (63)$$

To ensure the negativity of the term 1:

$$\begin{aligned} \frac{\gamma_1}{8\alpha^2} & > \frac{\|\zeta_c(t+1)\|^2}{\|\zeta_c(t)\|^2} \\ & = \frac{\|\tilde{w}^{(2)}(t)\|^2 \left(\|\phi(x(t))\|^2 + \|L\Delta x(t)\|^2 \right)}{\|\tilde{w}^{(2)}(t)\|^2 \|\phi(x(t))\|^2} \\ & = \frac{\|\phi(x(t))\|^2 + \|L\Delta x(t)\|^2}{\|\phi(x(t))\|^2} \\ & = 1 + \frac{\|L\Delta x(t)\|^2}{\|\phi(x(t))\|^2} \end{aligned} \quad (64)$$

where $\Delta x(t) = x(t+1) - x(t)$. The term $\frac{\|L\Delta x(t)\|^2}{\|\phi(x(t))\|^2}$ is the effect of the state transition from $x(t), x(t+1)$ on input to hidden layer of the critic, which can be proved to be upper bounded if $x(t), w_c^{(1)}(t)$ are upper bounded:

$$\begin{aligned} \frac{\|L\Delta x(t)\|^2}{\|\phi(x(t))\|^2} & \leq \frac{\|L\|^2 \|\Delta x(t)\|^2}{\|\tanh(w_c^{(1)}(t)x(t))\|^2} \\ & \leq \frac{\|w_c^{(1)}(t)x(t)\|^2 \|\Delta x(t)\|^2}{\|\tanh(w_c^{(1)}(t)x(t))\|^2} \\ & \leq \frac{\|\bar{w}_c^{(1)}(t)\bar{x}(t)\|^2 \|\Delta \bar{x}(t)\|^2}{\|\tanh(\bar{w}_c^{(1)}(t)\bar{x}(t))\|^2} \\ & = \delta \end{aligned} \quad (65)$$

given the monotonicity of $y = \frac{|x|^2}{|\tanh(x)|^2}$. $\|\Delta \bar{x}(t)\|$ is the upper bound of $\|\Delta x(t)\|$ and determined by the system dynamics and the length of discrete time step.

To ensure negativity of the term 2:

$$1 - l_c \|\phi_c(t)\|^2 - \frac{l_c}{\gamma_2} \|a(t)\|^2 \|y(t)\|^2 - \frac{1}{\gamma_2} > 0 \quad (66)$$

Therefore,

$$l_c < \min_t \frac{\gamma_2 - 1}{\gamma_2 (\|\phi_c(t)\|^2 + \frac{1}{\gamma_2} \|a(t)\|^2 \|y(t)\|^2)} \quad (67)$$

In particular, $\gamma_2 > 1$.

Similarly, to ensure negativity of the term 3:

$$\frac{1}{\gamma_1} - \frac{l_a}{\gamma_1} \|C(t)\|^2 \|\phi_a(t)\|^2 - \frac{l_a}{\gamma_3} \|D(t)C^T\|^2 \|x(t)\|^2 - \frac{1}{\gamma_3} > 0 \quad (68)$$

Therefore,

$$l_a < \min_t \frac{\gamma_3 - \gamma_1}{\gamma_3 \|C(t)\|^2 \|\phi_a(t)\|^2 + \gamma_1 \|D(t)C^T\|^2 \|x(t)\|^2} \quad (69)$$

In particular, $\gamma_3 > \gamma_1$.

The fourth term can be bounded as

$$\|w_c^{*(2)} \phi_c(t) - r(t) - \alpha \hat{w}_c^{(2)}(t) \phi_c(t+1)\|^2 \leq 4 \|w_c^{*(2)} \phi_c(t)\|^2 + 4r^2(t) + 2\alpha^2 \|\hat{w}_c^{(2)}(t) \phi_c(t+1)\|^2 \quad (70)$$

Let $\bar{C}, \bar{w}_{a1}, \bar{w}_{a2}, \bar{w}_{c1}, \bar{\phi}_a, \bar{y}, \bar{x}, \bar{a}, \bar{D}$ be upper bounds of $C, w_{a1}, w_{a2}, w_{c1}, \phi_a, y, x, a, D$, and let $w_{c2} = \max\{w_c^{*(2)}, w_{c2}^{(M)}\}$, where $w_{c2}^{(M)}$ is the upper bound of $\hat{w}_c^{(2)}(t)$. Finally, we obtain the following bound:

$$\begin{aligned} & \|w_c^{*(2)} \phi_c(t) - r(t) - \alpha \hat{w}_c^{(2)}(t) \phi_c(t+1)\|^2 + 4 \|r(t)\|^2 + \frac{8\alpha^2}{\gamma_1} \|w_c^{*(2)}(t) \phi_c(t+1)\|^2 + \frac{1}{\gamma_1} \|C(t)\|^2 \|\zeta_a(t)\|^2 \\ & + \frac{1}{\gamma_2} \|a(t)\|^2 \|\tilde{w}_c^{(1)}(t) y(t)\|^2 + \frac{1}{\gamma_3} \|C^T(t) D(t)\|^2 \|\tilde{w}_a^{(1)}(t) x(t)\|^2 \\ & \leq \left(\frac{8\alpha^2}{\gamma_1} + 4 + 2\alpha^2 \right) (\bar{w}_{c2} \bar{\phi}_c)^2 + 8\bar{r}^2 + \frac{1}{\gamma_1} (\bar{w}_{c2})^2 \bar{C} \bar{w}_{a2} \bar{\phi}_a^2 + \frac{1}{\gamma_2} (\bar{w}_{c1} \bar{y} \bar{a})^2 + \frac{1}{\gamma_3} (\bar{w}_c^{(2)} \bar{C} \bar{D} \bar{w}_{a1} \bar{x})^2 = M \end{aligned} \quad (71)$$

The conclusion is, if $\gamma_1 > 8\alpha^2(1 + \frac{\|L\Delta x(t)\|^2}{\|\phi(x(t))\|^2}) \|\zeta(t)\|^2$ in the term 1, and l_c, l_a satisfying (67), 69, and $\|\tilde{w}_c^{(2)}(t)\|^2 > \frac{M}{\|\phi(x(t))\|^2 - \frac{8\alpha^2}{\gamma_1} \|\phi(x(t+1))\|^2}$, we obtain $\Delta L(t) < 0$. Based on Theorem 1, this implies that the system of estimation errors is ultimately uniformly bounded. \square

VI. FLIGHT CONTROL SIMULATION

This section introduces an online reinforcement learning framework for angle-of-attack tracking control. A cascaded control structure is employed for separate control of angle-of-attack tracking and pitch rate tracking [20], [22]. The learning process is a sample-based implementation of the optimization-based tracking control design in Section ???. The learning algorithm uses Incremental model-based heuristic dynamic programming (IHDP).

A. Aerial Vehicle Model

The dynamical model of aerial vehicles is given as [32]

$$\begin{aligned} \dot{\alpha} &= \left(\frac{fgQS}{WV} \right) \cos(\alpha) [\phi_z(\alpha) + b_z \delta] + q \\ \dot{q} &= \left(\frac{fQSD}{I_{yy}} \right) [\phi_m(\alpha) + b_m \delta] \end{aligned} \quad (72)$$

where α is the angle of attack, q is the pitch rate, δ is the control surface deflection. The aerodynamic coefficients are approximately computed by $b_z = -0.034, b_m = -0.206$, and

$$\begin{aligned} \phi_z(\alpha) &= 0.000103\alpha^3 - 0.00945\alpha|\alpha| - 0.170\alpha \\ \phi_m(\alpha) &= 0.000215\alpha^3 - 0.0195\alpha|\alpha| - 0.051\alpha \end{aligned} \quad (73)$$

These approximations of $b_z, b_m, \phi_z(\alpha), \phi_m(\alpha)$ hold for α in the range of ± 20 degrees. The physical coefficients are provided in Table I. In addition, the actuator dynamics are considered as a first order model with the time constant 0.005s. The rate limit is 600 deg/s, and a control surface deflection limit is ± 20 degrees.

TABLE I: Physical parameters (adapted from [32])

Notations	Definition	Value
g	acceleration of gravity	9.815 m/s ²
W	weight	204.3 kg
V	speed	947.715 m/s
I_{yy}	pitch moment of inertia	247.438 kg·m ²
f	radians to degrees	180/π
Q	dynamic pressure	29969.861 kg/m ²
S	reference area	0.041 m ²
d	reference diameter	0.229 m

B. Tracking errors dynamics

Define the tracking errors as $e_1 = \alpha - \alpha_{\text{ref}}$, $e_2 = q - q_{\text{ref}}$, one has

$$\begin{aligned} \dot{e}_1 &= \dot{\alpha} - \dot{\alpha}_{\text{ref}} \\ &= f_1(x_1) + x_2 + d_1 - \dot{\alpha}_{\text{ref}} \\ &= f_1(x_1) + e_2 + q_{\text{ref}} + d_1 - \dot{\alpha}_{\text{ref}} \end{aligned} \quad (74)$$

$$\begin{aligned} \dot{e}_2 &= \dot{q} - \dot{q}_{\text{ref}} \\ &= f_2(x_1) + g_2 u - \dot{q}_{\text{ref}} \end{aligned} \quad (75)$$

where α_{ref} , q_{ref} are the angle-of-attack reference and the pitch rate reference. where $[x_1, x_2]^T = [\alpha, q]^T$, $u = \delta$ are state and control input. The nonlinear functions are defined as

$$\begin{aligned} f_1(x_1) &= \left(\frac{fgQS}{WV} \right) \cos(\alpha) \phi_z(\alpha), \quad d_1(x_1, u) = \left(\frac{fgQS}{WV} \right) \cos(\alpha) b_z \\ f_2(x_1) &= \left(\frac{fQSD}{I_{yy}} \right) \phi_m(\alpha), \quad g_2(x_1, \delta) = \left(\frac{fQSD}{I_{yy}} \right) b_m \end{aligned} \quad (76)$$

The model ?? is a single-input-single-output (SISO) system, as it has a single input that controls the state x_2 and subsequently influence the state x_1 through near-integrator dynamics, which exhibits dynamical oscillations when rate control is loose. The additional aerodynamic dynamics $f_1(\cdot)$ also disturb the angle-of-attack tracking error and the resulting control actions.

The virtual control defined as $q_{\text{ref}}(e_1, \alpha, \delta)$ is associated with e_1, α, δ , aiming to provide error-feedback control for stabilizing e_1 and from the intuitive point of view, compensate for the dynamics associated with α and δ in e_1 -subsystem. In backstepping this nominal model is used to design the virtual control and its adaptive variants to ensure asymptotic convergence of the tracking errors under model uncertainties. In model-free RL settings, the design of $q_{\text{ref}}(e_\alpha, \alpha, \delta)$ with guaranteed performance is infeasible as the dynamics are unknown. It is usually parameterized using a neural network and trained with samples. The same analysis applies to the design of u in e_2 -subsystem. The control surface deflection $\delta = u(e_2, q, \alpha)$ is a function of e_2, q and α , in order to stabilize e_2 and compensate for the dynamics associated with q, α .

C. Outer-loop and inner-loop agent

1) *Incremental model*: The incremental model of q -dynamics is developed as

$$\Delta q_{t+1} = F_{t-1} \Delta q_t + G_{t-1} \Delta \delta_t \quad (77)$$

where the subscript t denotes the discrete-time index. The state increments are defined as $\Delta q_{t+1} = q_{t+1} - q_t$, $\Delta q_t = q_t - q_{t-1}$, the control increment is defined as $\Delta \delta_t = \delta_t - \delta_{t-1}$. The first-order partial derivatives are $F_{t-1} = \frac{\partial f_2}{\partial \alpha} |_{\alpha_{t-1}, \delta_{t-1}, q_{t-1}}$, $G_{t-1} = \frac{\partial g_2 u}{\partial \delta_t} |_{\alpha_{t-1}, \delta_{t-1}, q_{t-1}}$. The derivation is seen in Appendix VIII-A. In practice, the model is identified using linear Recursive Least Squares algorithm (Appendix VIII-B).

Remark 5. The incremental model of the α -dynamics is not required during the training of the outer-loop actor, even though its task is to control angle-of-attack. This control effectiveness from q to α is implicitly captured in the estimated value function $\hat{V}_2(\cdot)$ by taking q as an input.

2) *Networked control laws*: The outer-loop control law and inner-loop control laws are parameterized using two neural networks as $q_{\text{ref}}(e_1, \alpha, \delta) = W_1(e_1, \alpha, \delta)$, $\delta(e_2, q, \alpha) = W_2(e_2, q, \alpha)$. The nested control law is

$$\delta(e_2, q, \alpha) = W_2(q - \underbrace{W_1(e_1, \alpha, \delta)}_{\text{outer-loop actor}}, q, \alpha) \quad (78)$$

inner-loop actor

where $W_1(\cdot; w^{A_1})$, $W_2(\cdot; w^{A_2})$ are neural networks with trainable parameter sets w^{A_1} , w^{A_2} . The cascaded structure is illustrated in Figure 1, along with a comparison to the monolithic actor.

3) *Outer-loop agent*: The outer-loop agent aims to learn a sub-optimal policy for pitch rate reference required to track the angle-of-attack reference. The network structures are shown in Figure ???. The critic takes angle-of-attack, its tracking error and pitch rate as inputs. The output is the estimated state-value $\hat{V}_{1(t)}$. The absolute-value function $\text{abs}(\cdot)$ is applied at the output layer to ensure positive definiteness. The actor uses control surface deflection as an additional input to attenuate the non-minimum phase dynamics. Its output is constrained using a scaled $\tanh(\cdot)$ function to satisfy the limits on the pitch-rate reference.

The critic is updated through TD learning to minimize a loss function:

$$L_t^{C_1} = \frac{1}{2} \delta_{1(t)}^T \delta_{1(t)} \quad (79)$$

where $\delta_{1(t)} = c_{1(t)} + \gamma \hat{V}_{1, \text{target}(t+1)} - \hat{V}_{1(t)}$ is the TD error, $\hat{V}_{1, \text{target}}(\cdot)$ is a target critic used to delay weight updates and stabilize the learning process.

The gradient of $L_t^{C_1}$ with respect to critic weights is

$$\frac{\partial L_t^{C_1}}{\partial w_t^{C_1}} = \frac{\partial L_t^{C_1}}{\partial \delta_{1(t)}} \frac{\partial \delta_{1(t)}}{\partial w_t^{C_1}} = -\delta_{1(t)} \frac{\partial \hat{V}_{1(t)}}{\partial w_t^{C_1}} \quad (80)$$

The critic is updated by stepping in opposite direction to the gradient of the loss with learning rate $\eta_t^{C_1}$:

$$w_t^{C_1} = w_t^{C_1} - \eta_t^{C_1} \frac{\partial L_t^{C_1}}{\partial w_t^{C_1}} \quad (81)$$

4) *Inner-loop agent*: The inner-loop agent aims to learn a sub-optimal policy for control-surface deflection required to track the pitch-rate reference. The non-minimum-phase dynamics associated with δ may unintentionally affect the α -dynamics. This is a key motivation for adopting a cascaded control structure, which isolates this effect from the inner-loop agent's training process. As a result, the outer-loop agent is prevented from attempting to control angle-of-attack through the control-surface deflection directly.

Figure ??? shows the network structures as single-hidden-layer fully-connected multi-layer-perceptions (MLP). The inputs of the critic are the pitch rate and the its tracking error. The output is the estimated state-value $\hat{V}_{2(t)}$. An absolute-value function $\text{abs}(\cdot)$ is applied at the output layer to ensure the positive definiteness. The actor uses angle-of-attack as an additional input to attenuate dynamic coupling in the q -dynamics. The output is the control surface deflection. A scaled $\tanh(\cdot)$ is applied at the output layer to constrain the action within actuator limits. The target critic and target actor share the same structures.

The critic is updated through Temporal Difference (TD) learning to minimize a loss function:

$$L_t^{C_2} = \frac{1}{2} \delta_{2(t)}^T \delta_{2(t)} \quad (82)$$

where $\delta_{2(t)} = c_{2(t)} + \gamma \hat{V}'_{2(t+1)} - \hat{V}'_{2(t)}$ is the TD error, $\hat{V}'_2(\cdot)$ denotes the target critic, which is updated as a delayed version of $\hat{V}_2(\cdot)$ to stabilize policy learning.

The gradient of the critic's loss with respect to its parameter vector is

$$\frac{\partial L_t^{C_2}}{\partial w_t^{C_2}} = \frac{\partial L_t^{C_2}}{\partial \delta_{2(t)}} \frac{\partial \delta_{2(t)}}{\partial w_t^{C_2}} = \delta_{2(t)} - \frac{\partial \hat{V}'_{2(t)}}{\partial w_t^{C_2}} \quad (83)$$

The critic is updated by

$$w_{t+1}^{C_2} = w_t^{C_2} - \eta_t^{C_2} \frac{\partial L_t^{C_2}}{\partial w_t^{C_2}} \quad (84)$$

The target critic is updated by

$$w_{t+1}^{C'_2} = \tau w_t^{C_2} + (1 - \tau) w_t^{C'_2} \quad (85)$$

5) *Actor*: The actor is trained to minimize the estimated state-value function:

$$L_t^{A_2} = c_{2(t)} + \gamma \hat{V}'_{2(t+1)} \quad (86)$$

$$\delta_t^* = \arg \min_{\delta_t} L_t^{A_2} \quad (87)$$

The gradient of the actor's loss with respect to its parameter vector is

$$\begin{aligned} \frac{\partial L_t^{A_2}}{\partial w_t^{A_2}} &= \frac{\partial L_t^{A_2}}{\partial \delta_t} \frac{\partial \delta_t}{\partial w_t^{A_2}} \\ &= \left(2b\delta_t + \frac{\partial \hat{V}'_2(e_{t+1}, q_{t+1}, \alpha_{t+1})}{\partial q_{t+1}} \frac{\partial q_{t+1}}{\partial \delta_t} \right) \frac{\partial \delta_t}{\partial w_t^{A_2}} \\ &= \left(2b\delta_t + \frac{\partial \hat{V}'_2(e_{t+1}, q_{t+1}, \alpha_{t+1})}{\partial q_{t+1}} \hat{G}_{t-1} \right) \frac{\partial \delta_t}{\partial w_t^{A_2}} \end{aligned} \quad (88)$$

The actor is updated by

$$w_{t+1}^{A_2} = w_t^{A_2} - \eta_t^{A_2} \frac{\partial L_t^{A_2}}{\partial w_t^{A_2}} \quad (89)$$

6) *Training*: The forward propagation of action q_{ref} goes through the inner-loop actor to generate an action δ that interacts with the model, seen as an additional control effectiveness. This implies that the outer-loop actor is equivalently interacting with an extended model that includes the inner-loop actor (see Figure 1). The training sample is given by $(e_{1(t)}, \alpha_t, q_t, \delta_t, q_{\text{ref}}, e_{1(t+1)}, \alpha_{t+1}, q_{t+1})$. Therefore, the gradient of the outer-loop actor propagates from $\hat{V}'_{1(t+1)}$ and back through the inner-loop actor. The training of the inner-loop actor is independent of the outer-loop actor, since the target critic $\hat{V}'_{2(t+1)}$ propagates gradients only to the inner-loop actor. Therefore, the samples $e_{1(t)}, e_{1(t+1)}$ are not used during training. The training sample is given by $(e_{2(t)}, q_t, \alpha_t, \delta_t, e_{2(t+1)}, q_{t+1})$. In this setting, the environment is treated as only the e_2 -dynamics.

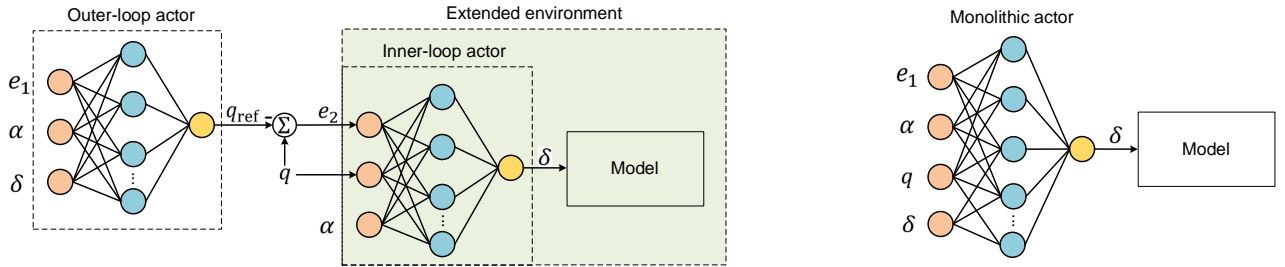


Fig. 1: Cascaded actor versus monolithic actor. The former uses an outer-loop actor to generate a pitch-rate reference, which is then passed to an inner-loop actor that produces the control-surface deflection, providing an explicit mechanism for learning and tracking the pitch-rate reference. The latter is a fully connected multilayer perceptron (MLP) that approximates an end-to-end tracking policy. The pitch-rate reference is not explicitly represented by the monolithic actor. This end-to-end structure is commonly used for the stabilization of inverted pendulum and Van der Pol's oscillator, without additional angular dynamics.

D. Action-smoothing techniques

This subsection introduces policy regularization for temporal smoothness technique and a low-pass filter to smoothen control actions. The first technique regularizes the actor to generate slow-varying actions, while the second technique filters the pitch rate reference.

1) *Policy regularization for temporal action smoothness*: The temporal action smoothness measure the extent to which the output changes when the actor input changes:

$$L_{1(t)}^{\text{TS}} = |q_{\text{ref}(t+1)} - q_{\text{ref}(t)}| \quad (90)$$

$$L_{2(t)}^{\text{TS}} = |\delta_{t+1} - \delta_t| \quad (91)$$

where $L_{1(t)}^{\text{TS}}, L_{2(t)}^{\text{TS}}$ are temporal smoothness (TS) losses for the outer-loop and inner-loop actors, respectively.

To reduce computation load in online learning, a single sample is used at each step of policy update to compute TS losses. This contrasts with using a minibatch in offline learning [29].

The multi-objective optimization frameworks are formulated as

$$q_{\text{ref}(t)}^* = \arg \min_{v_t} \left(c_{1(t)} + \gamma \hat{V}'_{1(t+1)} + \lambda_1 L_{1(t)}^{\text{TS}} \right) \quad (92)$$

$$\delta_t^* = \arg \min_{\delta_t} \left(c_{2(t)} + \gamma \hat{V}'_{2(t+1)} + \lambda_2 L_{2(t)}^{\text{TS}} \right) \quad (93)$$

where $\lambda_1 \geq 0, \lambda_2 \geq 0$ are weights of TS losses.

2) *Low-pass filter*: A second-order filter is used to smooth the pitch rate reference [30]:

$$\begin{aligned} \dot{d}_1 &= d_2 \\ \dot{d}_2 &= -2\zeta\omega_n d_2 - \omega_n^2 (d_1 - q_{\text{ref}}) \end{aligned} \quad (94)$$

where d_1, d_2 are filtered signal and its differentiation, ω_n is the natural frequency, ζ is the damping factor.

Remark 6. The training samples are collected under the Markov assumption for the environment, i.e., the one-step future state is determined solely by the current state. However, the states of the filter depend on the past two states due to its integral dynamics, which violates this assumption when a filter is used during the training of the outer-loop actor. As a result, the gradients from the value function \hat{V}_1 are delayed by two time steps due to the filter. This issue can be mitigated by including the filter states as part of the environment state; however, this increases computational cost because of the higher dimensionality of the system and network inputs. To avoid delaying the gradient, this paper excludes the filter from the backpropagation of the policy through \hat{V}_1 and applies it only during the forward propagation of the cascaded actor.

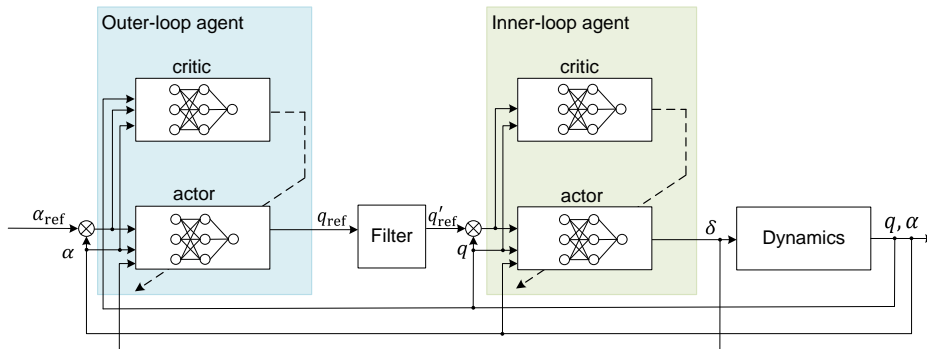


Fig. 2: Command-filtered cascaded online learning flight control system.

VII. SIMULATION

This section presents simulation results for cascaded online-learning flight control systems that incorporate action-smoothness conditioning techniques. The aerial vehicle dynamics are numerically simulated through the fourth-order Runge Kutta method. The actuator dynamics are modeled as a first-order system $\tau \dot{\delta}_t + \delta_t = \delta_{c(t)}, \tau = 0.005$. To constrain actions, the outer-loop and inner-loop actors are scaled to $[-20^\circ, 20^\circ]$ and $[-20^\circ/\text{s}, 20^\circ/\text{s}]$. The reference of angle-of-attack is set as $\alpha_{\text{ref}(t)} = 10^\circ \sin(\frac{2\pi}{T}t), T = 10\text{s}$. The network weights are randomly initialized using a uniform distribution $\mathcal{U}(-0.01, 0.01)$, which ensures an initially low-gain control law and slow learning to guard against inaccurate policy gradients. The persistence excitation signal is generated by adding Gaussian noise $\mathcal{N}(0, 0.04)$ to the control surface deflection. The hyperparameters of the RL agents are listed in Table II. The baseline control system does not use either of action-smoothing techniques. We consider the tracking control performance in aspects of tracking errors, action smoothness, saturation level of activation function, actor sensitivity and one-step costs.

TABLE II: Hyperparameters of RL agents

Parameter	Outer-loop agent	Inner-loop agent
critic learning rate η^{C1}, η^{C2}	0.1	0.1
actor learning rate η^{A1}, η^{A2}	5×10^{-7}	10^{-7}
discount factor γ	0.6	0.6
delay factor τ	1	1
policy iteration number at each time step	3	3
hidden layer size	7	7
critic hidden-layer activation function	tanh	tanh
critic output layer activation function	abs	abs
actor activation function	tanh	tanh
optimizer	Adam	Adam
control effort weights a, b	5×10^{-6}	10^{-5}
smoothness loss weight λ_1, λ_2	9.3×10^{-4}	10^{-5}
loss thresholds for terminating critic training	2.5×10^{-4}	5×10^{-5}
maximal steps of critic and actor updates	50	50

A. Temporal-smoothed control system

1) *Tracking control*: In Figure 3 the baseline control system exhibits satisfactory tracking performance during the first 10 seconds, but then experiences growing oscillations of the states and actions that degrade the convergence of the tracking error, ultimately leading to divergence. This issue is addressed in [Ref] by constraining the actions to the interval $[-5^\circ, 5^\circ]$, a hard constraint that does not prevent bang–bang control. In contrast, the temporal-smoothed control system produces smoother actions within $[-6^\circ, 6^\circ]$ and avoids both divergence and bang–bang behavior by penalizing temporal variations in the actions. Figure 4 shows that the critic parameters of both the two systems converge to their sub-optimum within 10s, but the former continues to oscillate in response to large tracking errors. The actor parameters in the temporal-smoothed system exhibit slightly slower growth thanks to the stabilized tracking errors.

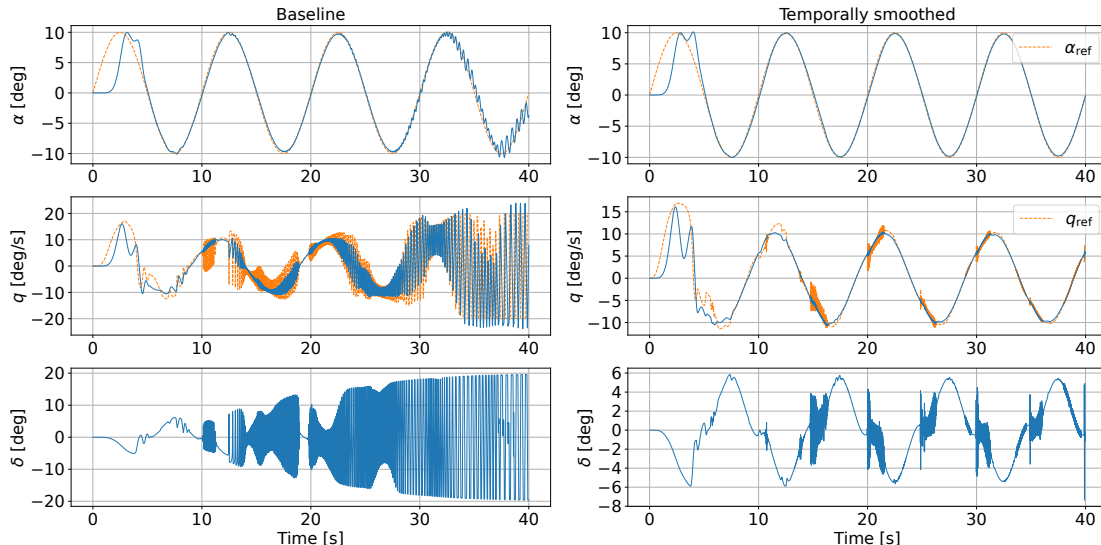


Fig. 3: Tracking control performance.

The frequency-domain characteristics of actions are captured by using the Fast Fourier Transform (FFT) algorithm, that converts the discrete-time action sequences into their frequency-domain representations, as given by the Discrete Fourier Transform $X[k] = \sum_{n=0}^{N-1} x[n] e^{-j\frac{2\pi}{N}kn}, k = 0, 1, \dots, N - 1$. Figures 5 and 6 show the time-domain histories and the spectra over the 0–100 Hz range. The signals of q_{ref} within 100 Hz are effectively attenuated using TS losses, and their amplitude of q_{ref} is significantly reduced without compromising tracking performance. Similar results are observed for control surface deflection. A reason for the oscillation of action δ is that a switching tracking error e_2 induced by the switching q_{ref} propagates through the lower-level actor to generate δ .

2) *Activation function*: The activation function $\tanh(\cdot)$ is saturated if its output approaches the maximum or minimum value due to large inputs. In the saturated region of $\tanh(\cdot)$, its gradient vanishes and approaches zero (see Figure 7). The vanishing derivative leads to a vanishing policy gradient, resulting in slow learning of the control policy. Another effect is that the actor produces actions near their maximum or minimum limits in response to small tracking errors, resulting in an almost bang–bang control law that degrades tracking performance and system stability.

The saturation of the actor is the result of an aggressive process of policy learning. This occurs for two main reasons: (1) a large learning rate. A large learning rate causes the actor’s weights to be updated with large increments, pushing the activation

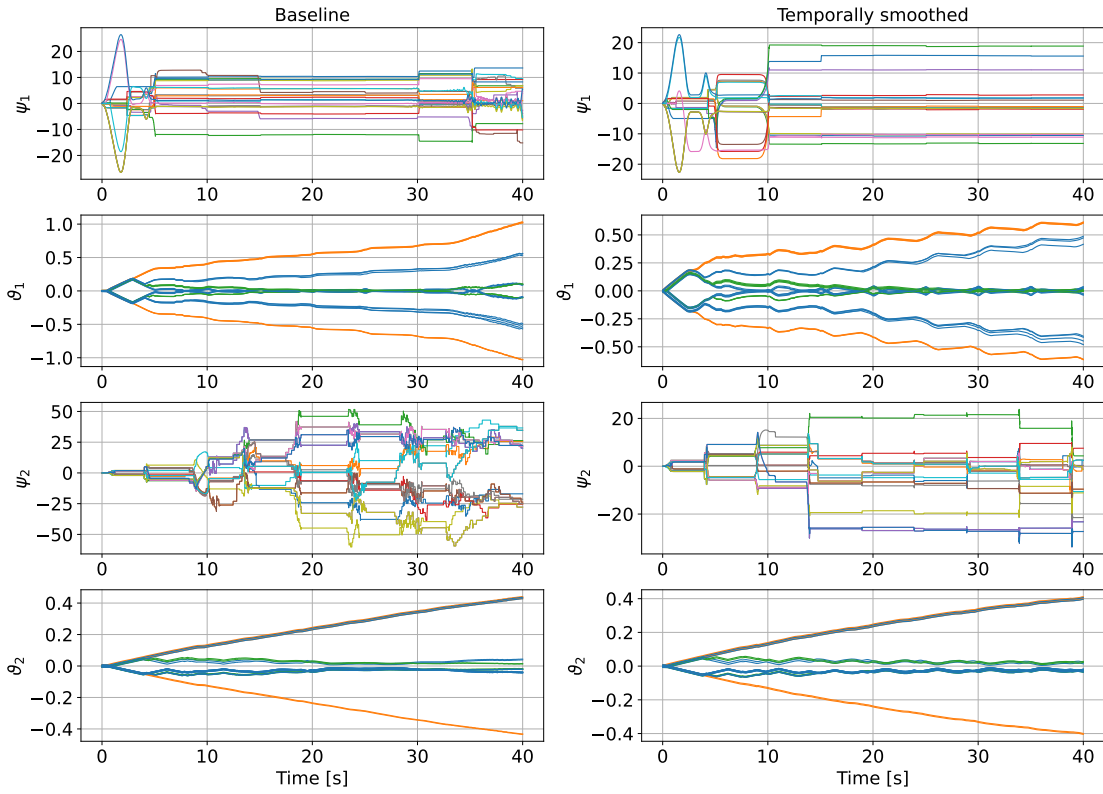


Fig. 4: Critic and actor parameters.

function into its saturation zone, a process that is irreversible due to vanishing gradients. (2) Underemphasized control effort in the one-step cost function. An one-step cost function that underemphasizes the control effort does not discourage the actor to use large actions during learning. The vanishing gradients make these aggressive actions stay and persist to degrade the tracking performance even as the tracking error decreases. Between 10 and 20s, although $\tanh(\cdot)$ is not saturated, significant switching actions occur, indicating that switching actions can happen even within the normal operating region of $\tanh(\cdot)$. Moreover, the time-varying dynamics and reference cause switching tracking errors, which propagate to the pitch-rate reference and control surface deflections through the cascaded actor.

Figure 7 shows the saturation level of $\tanh(\cdot)$ in output layers of actors. The baseline control system eventually makes the inputs reach to intervals $[-4,-2]$, $[2,4]$ (the outer-loop actor) and intervals $[-3,-2]$, $[2,3]$ (the lower-level actor). In these intervals, the derivative is $\tanh'(\cdot) \leq 0.1$ and attenuates the overall policy gradient. As a comparison, the temporal-smoothed control system avoids reaching to the saturation regions. The inputs are kept within 'unsaturated' interval $[-2,2]$ (the outer-loop actor) and interval $[-0.5,0.5]$ (the lower-level actor). This demonstrates the effectiveness of TS losses in avoiding saturation of $\tanh(\cdot)$.

3) *Action increment*: The one-step increment of pitch rate reference is

$$\Delta q_{\text{ref}(t+1)} = |q_{\text{ref}(t+1)} - q_{\text{ref}(t)}| \quad (95)$$

where $q_{\text{ref}(t+1)} = W_1(e_1(t+1), \alpha_{t+1}, \delta_{t+1})$, $q_{\text{ref}(t)} = W_1(e_1(t), \alpha_t, \delta_t)$ are actors' outputs.

The one-step increment of control surface deflection is

$$\Delta \delta_{t+1} = |\delta_{t+1} - \delta_t| \quad (96)$$

where $\delta_{t+1} = W_2(e_2(t+1), q_{t+1}, \alpha_{t+1})$, $\delta_t = W_2(e_2(t), q_t, \alpha_t)$ are actors' outputs .

Figure 8 shows the baseline control system suffers from fast-switching actions. Using a TS loss reduces the amplitude of the action increment to $|\Delta q_{\text{ref}(t+1)}| \leq 0.5$ °s and decreases the amplitude of $|\Delta \delta(t+1)|$, resulting in less saturated control actions.

4) *Actor sensitivity*: The sensitivity of the actor indicates how much, and in what direction, the output changes when the input increases slightly [34]. An actor with high sensitivity may overreact to its inputs, state variations and the tracking error. This is also correlated to robustness of the actor against sensor noise and uncertainties.

The sensitivity of the inner-loop and outer-loop actors is measured by

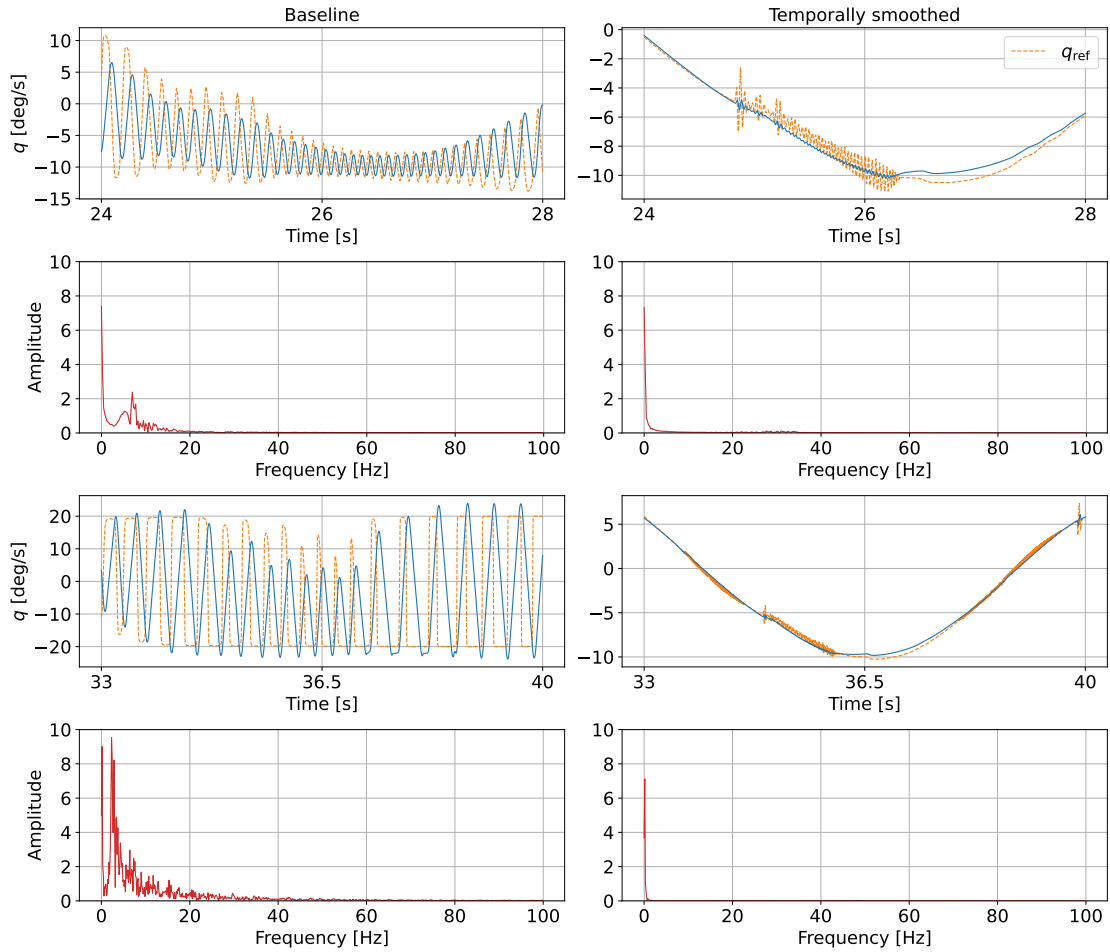


Fig. 5: Pitch rate in selected intervals.

$$K_{1(t)} = \frac{\partial q_{\text{ref}(t)}}{\partial e_{1(t)}} \quad (97)$$

$$K_{2(t)} = \frac{\partial \delta(t)}{\partial e_{2(t)}} \quad (98)$$

The relation between the pitch rate reference and its sensitivity measure is

$$\begin{aligned} & |q_{\text{ref}(t+1)} - q_{\text{ref}(t)}| \\ & \approx |K_{1(t)}(e_{1(t+1)} - e_{1(t)})| \\ & = |K_{1(t)}| \cdot |e_{1(t+1)} - e_{1(t)}| \end{aligned} \quad (99)$$

Similarly, the relation between the control surface deflection and its sensitivity measure is

$$\begin{aligned} & |\delta_{(t+1)} - \delta_{(t)}| \\ & \approx |K_{2(t)}(e_{2(t+1)} - e_{2(t)})| \\ & = |K_{2(t)}| \cdot |e_{2(t+1)} - e_{2(t)}| \end{aligned} \quad (100)$$

Equations 99, 100 show that the action increments can be reduced through reducing sensitivity.

In Figure 9, the fast-growing K_1, K_2 of the baseline control system indicate the actors are becoming significantly sensitive to variants of tracking errors. The oscillations are the results of actor saturation. The temporal-smoothed control system shows reduced oscillations because the TS losses penalize the increments of actions, which affects the actor sensitivity, as shown in Equations 99, 100.

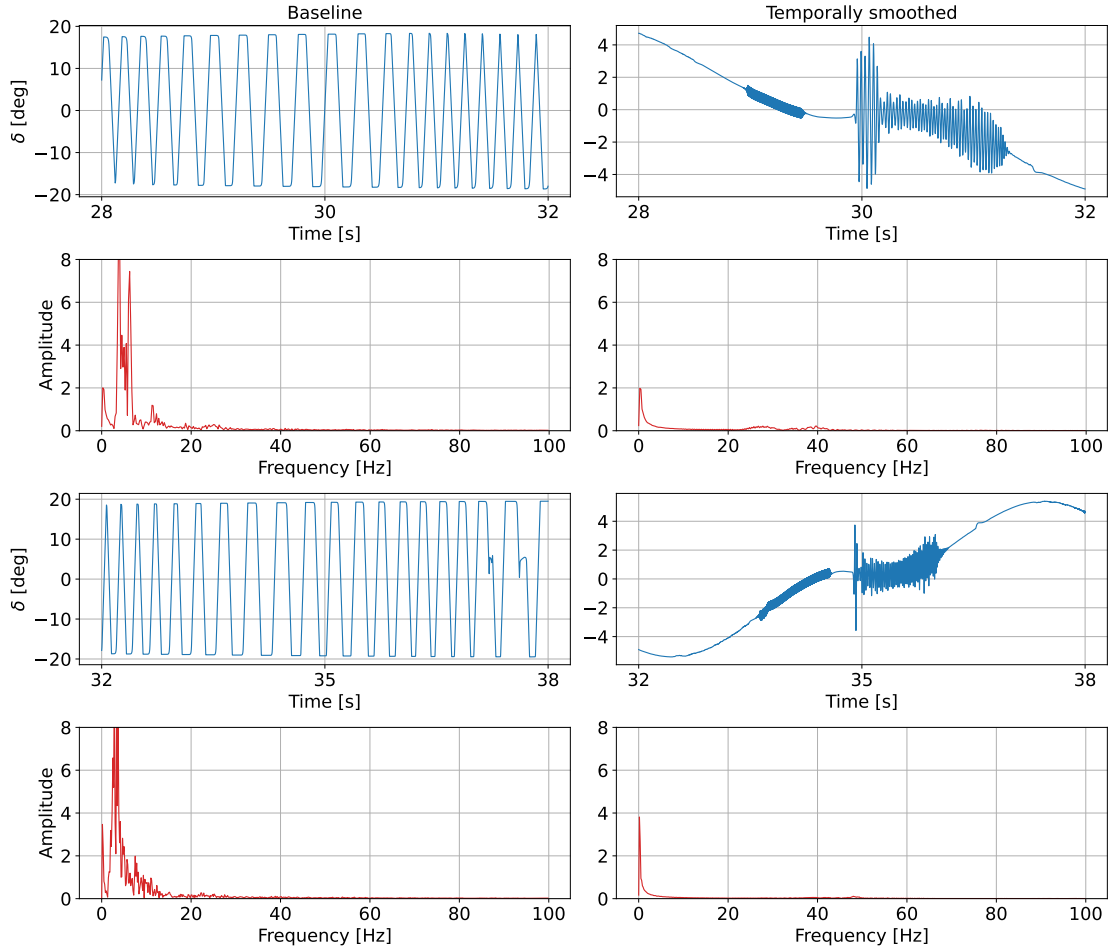


Fig. 6: Control surface deflection in selected intervals.

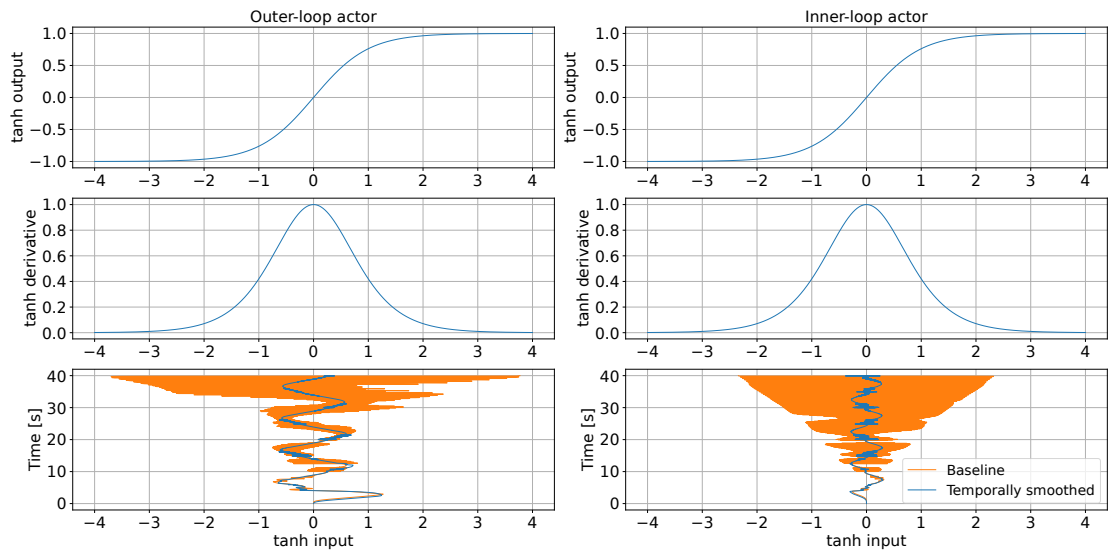


Fig. 7: Input of the activation function $\tanh(\cdot)$ in output layers of actors.

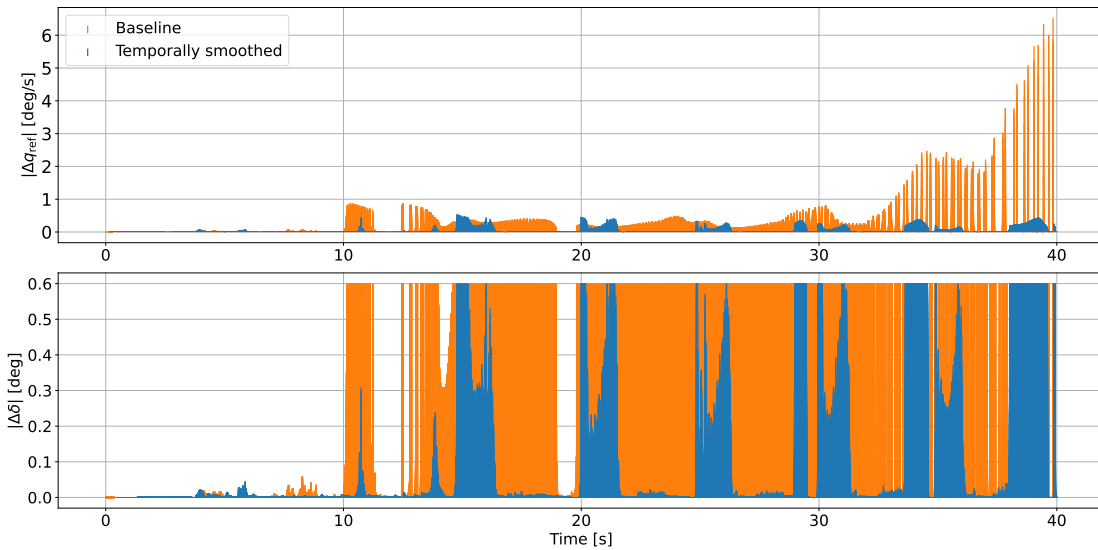


Fig. 8: Increments of actions.

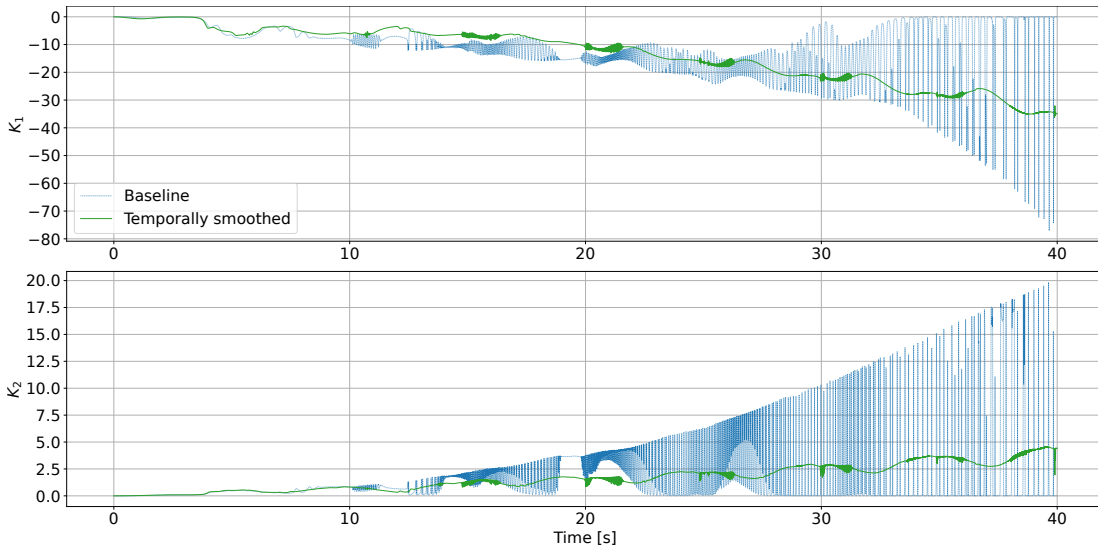


Fig. 9: Sensitivity measures.

5) *Challenges*: Although regularizing the policy using TS losses helps to generate smoother actions, the tuning of λ_1, λ_2 remains empirical. Large values slow down the process of policy learning, while small values degrade action smoothness effect. Moreover, Figure 10 shows that the TS losses do not eliminate low-amplitude, high-frequency oscillations in $\Delta q_{ref}(t+1)$ and $\Delta \delta_{ref}(t+1)$, since the penalization effects diminish when the increments are small (see Equations 90, 91). In this situation, a low-pass filter can be used, as it effectively removes high-frequency components from a frequency-domain perspective, thereby attenuating these action oscillations. Meanwhile, incorporating a low-pass filter into the flight control system does not interfere with the training process of actors.

B. Command-filtered and temporal-smoothed control system

We introduce a low-pass filter into the cascaded online learning flight control system, which has been demonstrated effective in filtering pitch rate reference in backstepping [5]. The natural frequency and damping ratio are $\omega_n = 20\text{rad/s}$ and $\zeta = 0.7$.

1) *Tracking control*: Figure 10 compares the temporal-smoothed control system with its counterpart that includes a filter. The amplitude of the control surface deflection oscillation exceeds that of the pitch-rate reference oscillation, due to the proportional amplification of e_2 by the inner-loop actor. The filter is capable of attenuating oscillations in pitch rate reference, leading to smooth e_2 and smooth control surface deflection through the inner-loop actor. Figure 11 presents detailed comparisons of q_{ref} over selected time periods. The q_{ref} signals in the 10-40Hz range are effectively attenuated by the filter. Figure 12 provides detailed comparisons on δ over selected time periods. The δ signals in the 10-40Hz range are effectively attenuated. These

observations account for the chosen filter parameters. Figure 13 shows the saturation level of $\tanh(\cdot)$ in the output layer of actors. Both control systems prevent saturation of $\tanh(\cdot)$, ensuring that its derivative satisfies $\tanh'(\cdot) \geq 0.4$ (the outer-loop actor) and $\tanh'(\cdot) \geq 0.8$ (the inner-loop actor). The comparisons on K_1, K_2 in Figure 14 show that applying a filter slows their growth and reduces oscillations, contributing to a more robust controller.

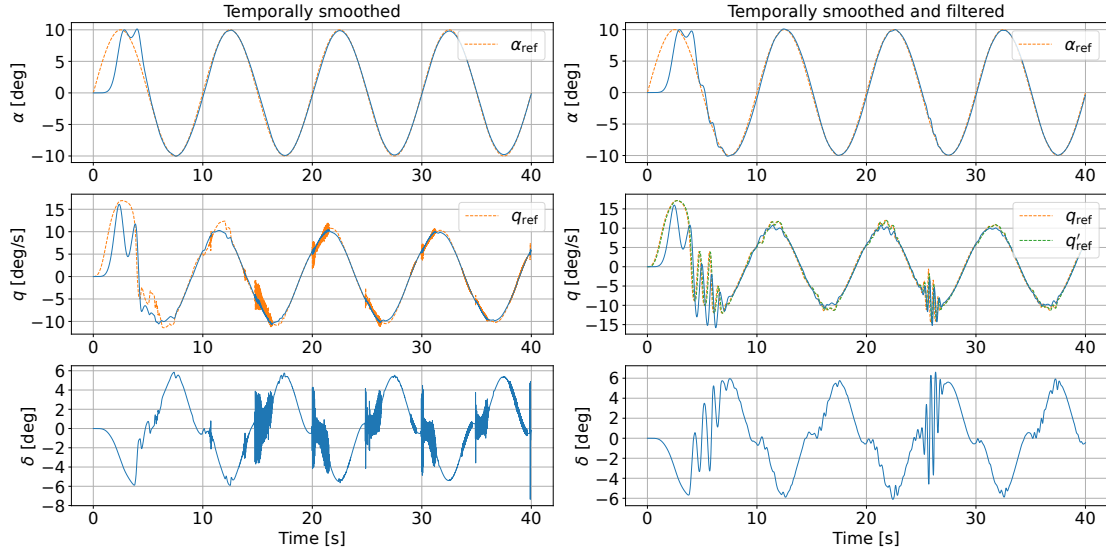


Fig. 10: Tracking performance comparison.

C. Terminate and restart learning

1) *Termination*: The previous analysis assumes continual learning; that is, the agents never terminate learning during system operation. The issue lies in that growing control gains can cause state oscillations, even when tracking errors are small. Therefore, it is intuitive to terminate and restart learning based on tracking performance over a recent time period. Specifically, the actor is fixed if the accumulated tracking error over a period T_s remains within a specified threshold:

$$\bar{e}_s \leq \epsilon \quad (101)$$

where $\bar{e}_s = \frac{1}{n_s} \sum_{i=0}^{n_s-1} |e_{t-i}|$ is the average of absolute tracking errors, $n_s = T_s/\Delta T$ is the number of samples, $\epsilon > 0$ is an error threshold. A large error threshold makes learning terminated early when tracking errors are still large. Define the online-learning state indicator as $\tau \in \{1, 0\}$, with $\tau = 1$ denoting that learning is off and $\tau = 0$ denoting that learning is on.

During the initial phase, when $t < T_s$ and there are not enough samples to compute \bar{e}_s , learning remains active:

$$\tau = 0, \text{ if } t < T_s \quad (102)$$

2) *Restart*: The learning must restart when the historical control performance degrades, typically occurring when the control system falls into faults and uncertainties. The restart condition determines in what case to restart learning. The evaluation period, denoted by T_r , should be carefully chosen to ensure it qualifies to represent the required control performance. A long evaluation period would delay the restart, preventing a timely response to performance degradation, while a short evaluation period makes the restart decision overly sensitive, potentially triggered by measurement noise or short-term peaks. As a result, the learning state may switch frequently between on and off.

The restart condition is

$$\bar{e}_r \geq \sigma \quad (103)$$

where $\bar{e}_r = \frac{1}{n_r} \sum_{i=0}^{n_r-1} |e_{t-i}|$ is the average of absolute tracking errors, $n_r = T_r/\Delta T$ is the number of samples, $\sigma > 0$ is an error threshold. The sketch maps are provided in Figure 15. The pseudocode is seen in Algorithm 1.

The outer-loop and inner-loop agents have independent termination and restart conditions. Their parameters are seen in Table III. Figure 16 shows the histories of average tracking errors and the indicators. The outer-loop agent is turned off at 29s and restarted at 31.5s, while the inner-loop agent is turned off at 22s and is never restarted.

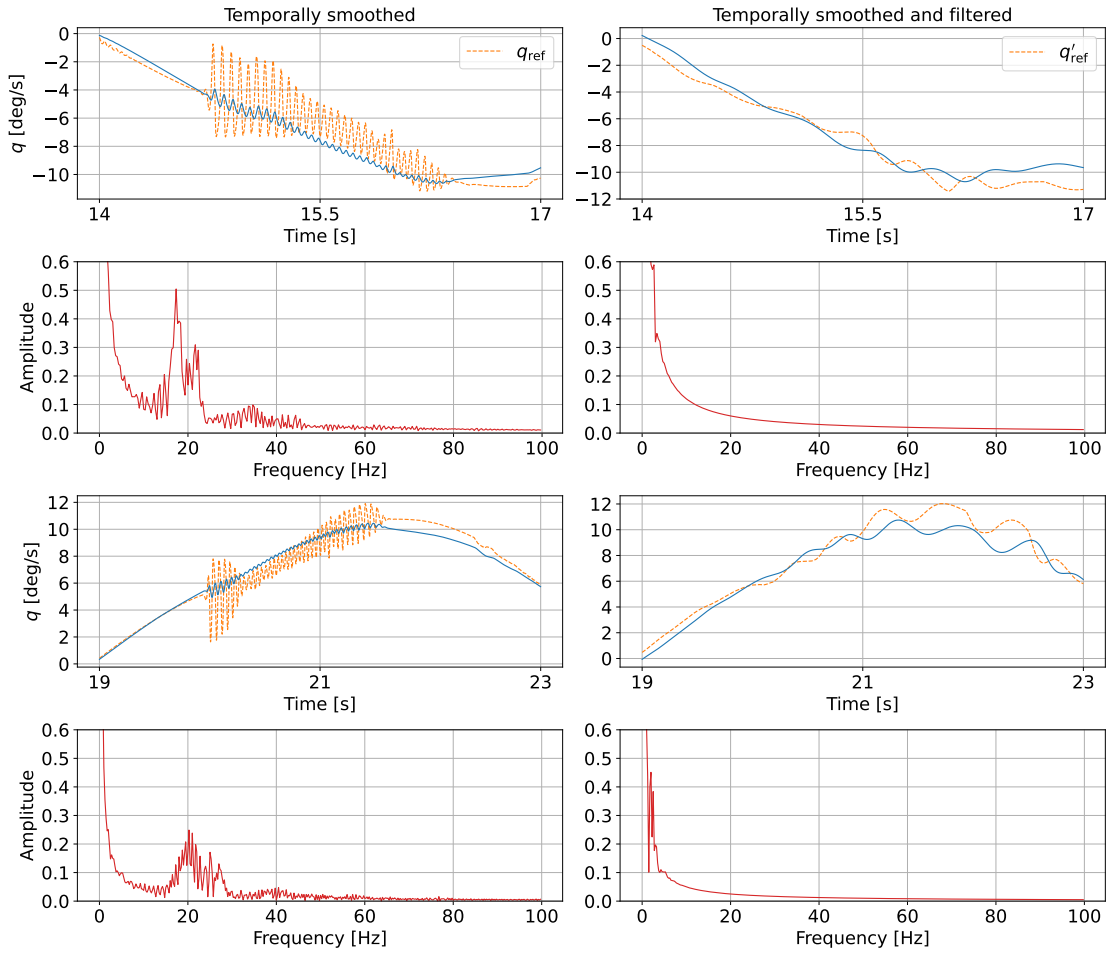


Fig. 11: Pitch rate in selected intervals.

Algorithm 1: Termination and restart algorithm

Data: $T_s, \epsilon, T_r, \sigma, t, \Delta T$

- 1 **Initialization** termination indicator $\tau_{-1} = 0$
- 2 **for each environment step** $t \leftarrow t_{max}$ **do**
- 3 **if** $\tau_{t-1} = 0$ **then**
- 4 **if** $t \leq T_s$ **then**
- 5 $\tau_t = 0$
- 6 **else**
- 7 **if** $\bar{e}_s \leq \epsilon$ **then**
- 8 $\tau_t = 1$
- 9 **else**
- 10 $\tau_t = 0$
- 11 **end**
- 12 **end**
- 13 **end**
- 14 **end**
- 15 **if** $\tau_{t-1} = 1$ **then**
- 16 **if** $\bar{e}_r \geq \sigma$ **then**
- 17 $\tau_t = 0$
- 18 **else**
- 19 $\tau_t = 1$
- 20 **end**
- 21 **end**

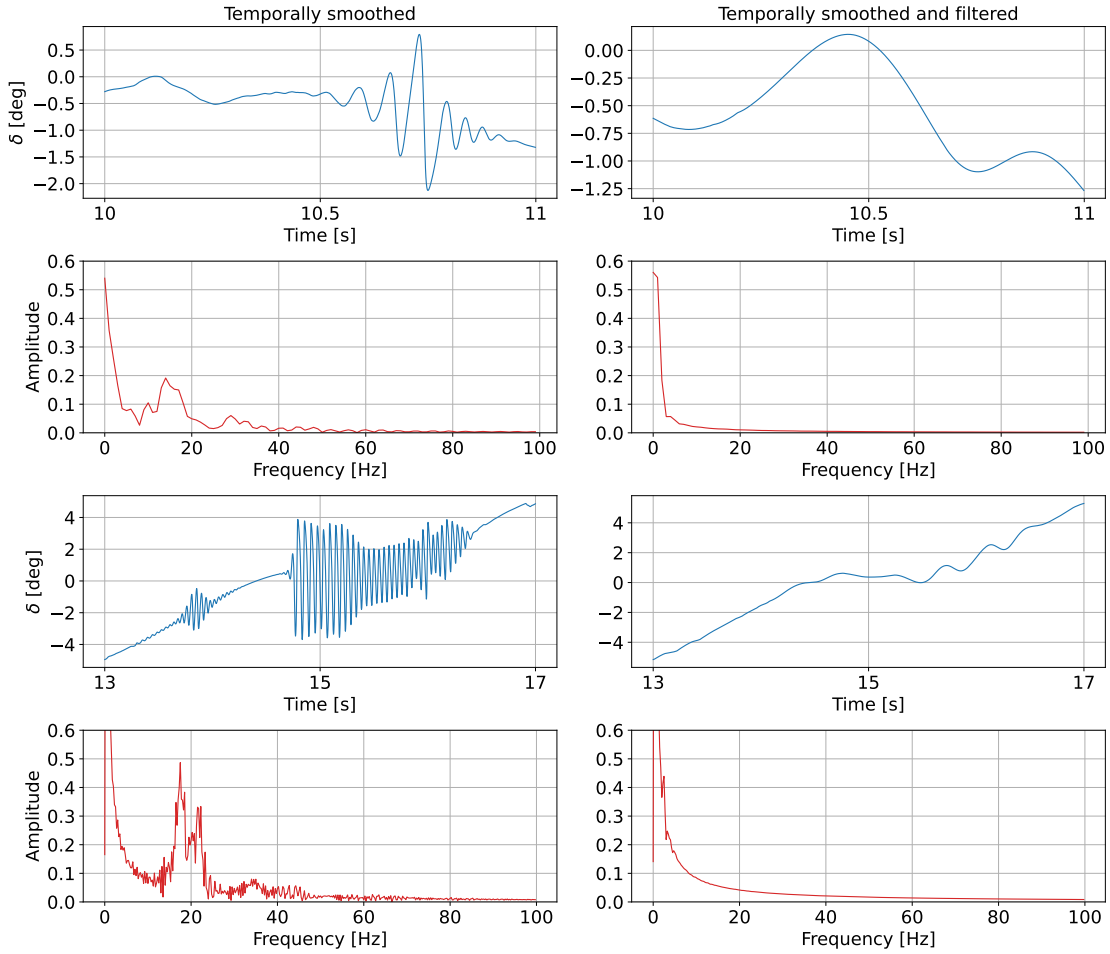


Fig. 12: Control surface deflection in selected intervals.

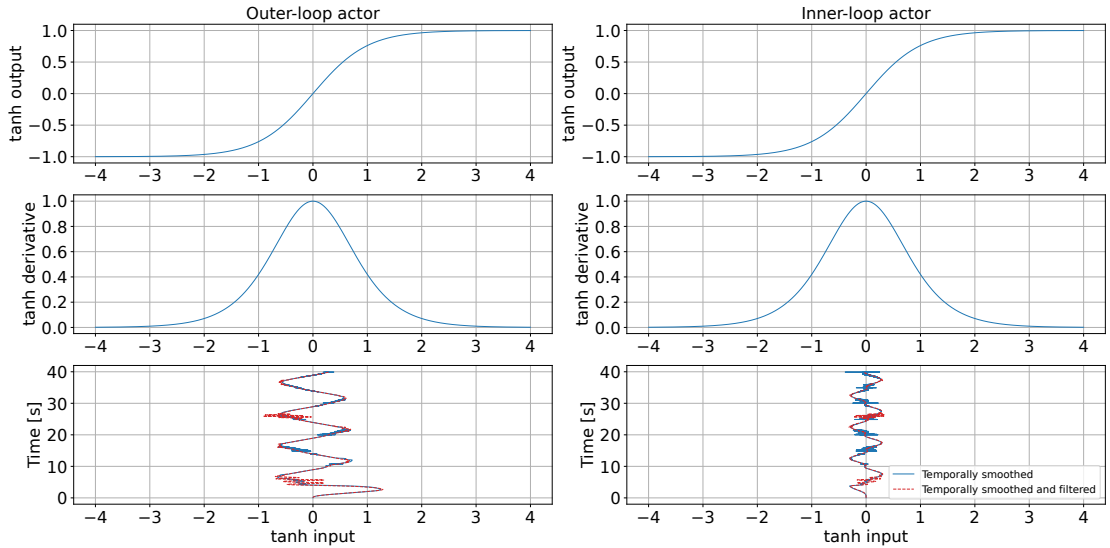


Fig. 13: Input of the activation function $\tanh(\cdot)$ in the output layer of actors.

TABLE III: Parameters

Parameter	Outer-loop agent	Inner-loop agent
T_s	10s	10s
ϵ	0.25°	0.5deg/s
T_r	0.2s	0.1s
σ	0.8°	2deg/s

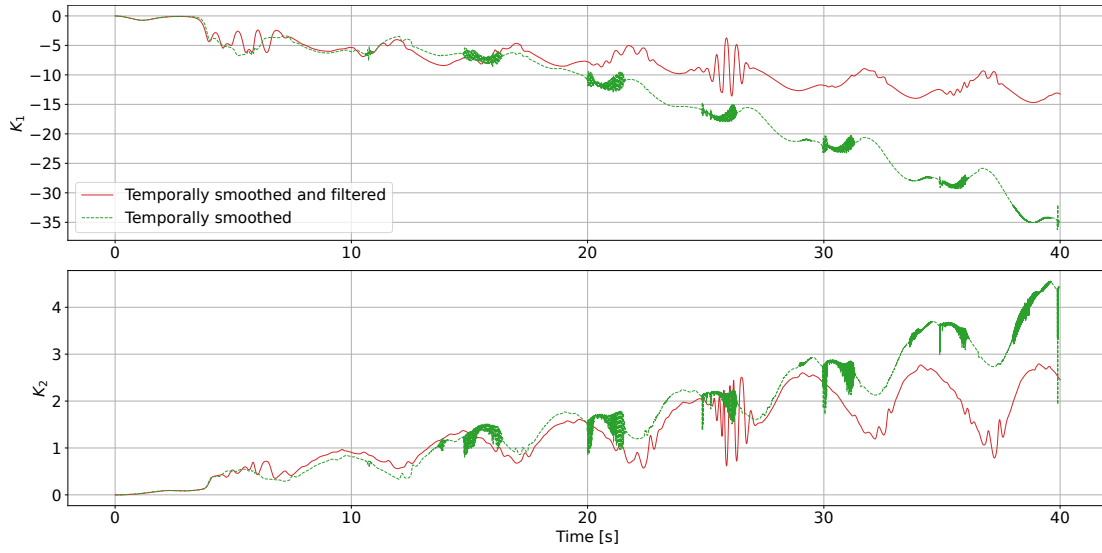


Fig. 14: Sensitivity measures.

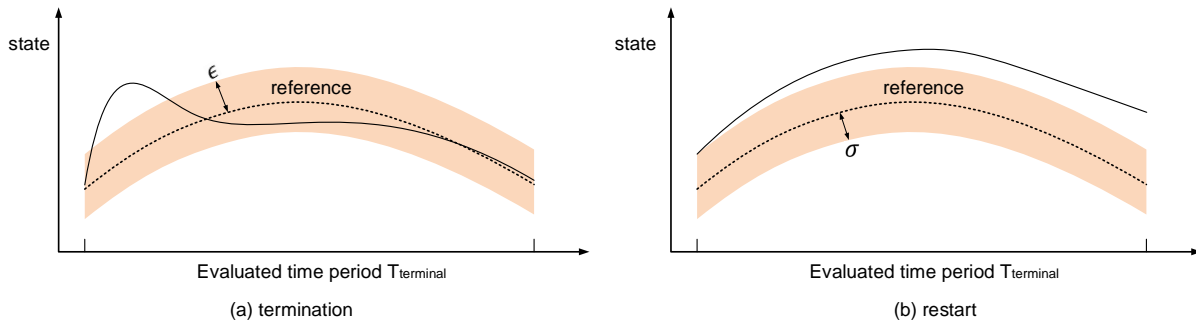


Fig. 15: Termination case (left) and restart case (right). The shaded area represents an average performance threshold. The actual average tracking errors must remain below this threshold to terminate learning, and exceed it to trigger a restart.

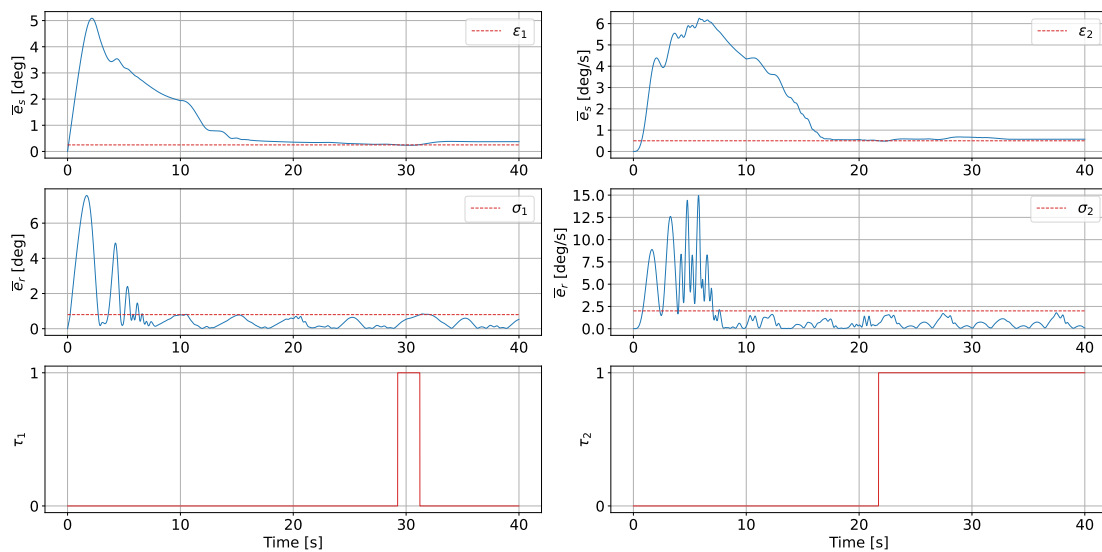


Fig. 16: Termination and restart measures.

VIII. CONCLUSION

We introduced two action-smoothing techniques into the cascaded online learning flight control system: temporal policy regularization and low-pass filter. The temporal policy regularization is verified through simulation to reduce the amplitude of pitch rate reference and control surface deflection. The low-pass filter is verified capable of removing the high-frequency signals of pitch rate reference, which cannot be accomplished by only using temporal policy regularization. The combination of these two methods enables a sufficient-level action smoothness during online learning. These techniques are necessary for online learning-based control of aerial vehicle systems with time-varying dynamics, suffering from oscillations of states and actions caused by switching tracking error.

APPENDIX

A. Derivation of incremental model

The continuous nonlinear system is given as

$$\dot{x}(t) = f(x(t), u(t)) \quad (104)$$

where the dynamics $f: \mathbb{R}^n \times \mathbb{R}^m \rightarrow \mathbb{R}^n$ is a smooth function associated with state vector $x \in \mathbb{R}^n$ and input vector $u \in \mathbb{R}^m$. n, m are positive integers denoting the dimensions of the state and action spaces.

Taking Taylor expansion for $f(x(t), u(t))$ at t_0 :

$$\begin{aligned} f(x(t), u(t)) &= f(x(t_0), u(t_0)) + F(t_0)(x(t) - x(t_0)) + G(t_0)(u(t) - u(t_0)) \\ &\quad + O[(x(t) - x(t_0))^2, (u(t) - u(t_0))^2] \end{aligned} \quad (105)$$

where $F(t_0) = \partial f(x, u)/\partial x|_{x(t_0), u(t_0)} \in \mathbb{R}^{n \times n}$, $G(t_0) = \partial f(x, u)/\partial u|_{x(t_0), u(t_0)} \in \mathbb{R}^{n \times m}$ are first-order partial derivatives at t_0 . $O(\cdot)$ is the summed higher-order terms.

The summed higher-order terms $O(\cdot)$ have a relatively small effect on the change from x_t to x_{t+1} compared with the first-order terms. Moreover, these higher-order derivatives are difficult to identify from data, which poses challenges for practical application of an incremental model that includes them. For these two reasons, we omit $O(\cdot)$ when defining an effective and practical model for the nonlinear system:

$$f(x(t), u(t)) = f(x(t_0), u(t_0)) + F(t_0)(x(t) - x(t_0)) + G(t_0)(u(t) - u(t_0)) \quad (106)$$

Using Equation 104:

$$\dot{x}(t) = \dot{x}(t_0) + F(t_0)[x(t) - x(t_0)] + G(t_0)[u(t) - u(t_0)] \quad (107)$$

The time derivatives are approximated by $\dot{x}(t) \approx \frac{x(t+T) - x(t)}{T}$ and $\dot{x}(t_0) \approx \frac{x(t_0+T) - x(t_0)}{T}$, where T is a constant time step. Then

$$\frac{x(t+T) - x(t)}{T} \approx \frac{x(t_0+T) - x(t_0)}{T} + F(t_0)[x(t) - x(t_0)] + G(t_0)[u(t) - u(t_0)] \quad (108)$$

Define a discretization approach over T by setting $t_0 = (k-1)T$, $x(t_0) = x((k-1)T) \triangleq x_{k-1}$. Let $x(t)$ denote the next-step state following $x(t_0)$, then $x(t) = x(t_0 + T) \triangleq x_k$.

A discretized version of system 108 is

$$x_{k+1} - x_k \approx x_k - x_{k-1} + F_{k-1}(x_k - x_{k-1})T + G_{k-1}(u_k - u_{k-1})T \quad (109)$$

Use denotions $\Delta x(k+1) = x(k+1) - x(k)$, $\Delta x(k) = x(k) - x(k-1)$, $\Delta u(k) = u(k) - u(k-1)$:

$$\Delta x_{k+1} = \Delta x_k + F_{k-1}\Delta x_k T + G_{k-1}\Delta u_k T \quad (110)$$

B. Recursive Least Squares identification

The linear forgetting Recursive Least Squares (RLS) algorithm is applied to identify matrices F_{t-1}, G_{t-1} are identified online. Define the augmented state as $\mathbf{x}_t = [\Delta q_t, \Delta \delta_t]^T$ and estimated parameter vector as $\hat{\theta}_{t-1} = [\hat{F}_{t-1}, \hat{G}_{t-1}]^T$. The one-step state prediction is made as $\Delta \hat{\mathbf{x}}_{t+1}^T = \mathbf{x}_t^T \hat{\theta}_{t-1}$. The error between the true state and the predicted state is denoted by ε_t and defined as $\varepsilon_t = \Delta \mathbf{x}_{t+1}^T - \Delta \hat{\mathbf{x}}_{t+1}^T$. The parameter matrix is updated by

$$\hat{\theta}_t = \hat{\theta}_{t-1} + P_t \mathbf{x}_t \varepsilon_t \quad (111)$$

$$\begin{aligned} P_t^{-1} &= \alpha P_{t-1}^{-1} + \mathbf{x}_t \mathbf{x}_t^T \\ &= \sum_{j=1}^t \alpha^{t-j} \mathbf{x}_j \mathbf{x}_j^T + \alpha^t P_0^{-1} \\ &= \sum_{j=1}^t \alpha^{t-j} \mathbf{x}_j \mathbf{x}_j^T + I \alpha^t \lambda_{\min}(0) \end{aligned} \quad (112)$$

The initial auxiliary matrix is set as $P_0 = I/\lambda_{\min}(0)$, where $0 < \lambda_{\min}(0) \ll 1$ is the minimum eigenvalue of P_0^{-1} . The initial parameter matrix is $\hat{\theta}_0$. The forgetting factor is $0 \ll \alpha < 1$.

REFERENCES

- [1] J. D. Anderson *Fundamentals of Aerodynamics*. McGraw-Hill Series in Aeronautical and Aerospace Engineering. New York, USA: McGraw-Hill, 2017.
- [2] S. Sieberling, Q. P. Chu, and J. A. Mulder Robust Flight Control Using Incremental Nonlinear Dynamic Inversion and Angular Acceleration Prediction *Journal of Guidance, Control and Dynamics*, vol. 33, no. 6, pp. 1732–1742, 2010, doi: 10.2514/1.49978.
- [3] X. R. Wang, E. van Kampen, Q. P. Chu and P. Lu Stability Analysis for Incremental Nonlinear Dynamic Inversion Control *Journal of Guidance, Control and Dynamics*, vol. 42, no. 5, pp. 1116–1129, 2019, doi: 10.2514/1.G003791.
- [4] Z. C. Liu, Y. F. Zhang, and J. J. Liang and H. X. Chen Application of the Improved Incremental Nonlinear Dynamic Inversion in Fixed-Wing UAV Flight Tests *Journal of Aerospace Engineering*, vol. 35, no. 6, pp. 1–13, 2022, doi: 10.1061/(ASCE)AS.1943-5525.0001495.
- [5] Y. C. Wang, W. S. Chen, S. X. Zhang, J. W. Zhu and L. J. Cao Command-Filtered Incremental Backstepping Controller for Small Unmanned Aerial Vehicles *Journal of Guidance, Control, and Dynamics*, vol. 41, no. 4, pp. 952–965, 2018, doi: 10.2514/1.G003001.
- [6] X. R. Wang, E. van Kampen, Q. P. Chu and P. Lu Incremental Sliding-Mode Fault-Tolerant Flight Control *Journal of Guidance, Control, and Dynamics*, vol. 42, no. 2, pp. 244–259, 2019, doi: 10.2514/1.G003497.
- [7] W. H. Chen, J. Yang, L. Guo and S. H. Li Disturbance-Observer-Based Control and Related Methods—An Overview *IEEE Transactions on Industrial Electronics*, vol. 63, no. 2, pp. 1083–1095, 2016, doi: 10.1109/TIE.2015.2478397.
- [8] D. M. Acosta and S. S. Joshi Adaptive Nonlinear Dynamic Inversion Control of an Autonomous Airship for the Exploration of Titan *AIAA Guidance, Navigation and Control Conference and Exhibit*, Hilton Head, South Carolina, USA, August, 2007, doi: 10.2514/6.2007-6502.
- [9] E. J. J. Smeur, Q. P. Chu and G. H. E. de Croon Adaptive Incremental Nonlinear Dynamic Inversion for Attitude Control of Micro Air Vehicles *Journal of Guidance, Control, and Dynamics*, vol. 39, no. 3, pp. 450–461, 2016, doi: 10.2514/1.G001490.
- [10] B. Smit, T. S. C. Pollack and E. van Kampen Adaptive Incremental Nonlinear Dynamic Inversion Flight Control for Consistent Handling Qualities *AIAA SciTech 2022 Forum*, San Diego, CA&Virtual, USA, January, 2022, doi: 10.2514/6.2022-1394.
- [11] J. Harris, C. M. Elliott and G. S. Tallant L1 Adaptive Nonlinear Dynamic Inversion Control for the Innovative Control Effectors Aircraft *AIAA SciTech 2022 Forum*, San Diego, CA&Virtual, USA, January, 2022, doi: 10.2514/6.2022-0791.
- [12] L. Sonneveldt, Q. P. Chu and J. A. Mulder Constrained Adaptive Backstepping Flight Control: Application to a Nonlinear F-16/MATV Model *AIAA Guidance, Navigation and Control Conference and Exhibit*, Keystone, Colorado, USA, August, 2006, doi: 10.2514/6.2006-6413.
- [13] L. Sonneveldt, Q. P. Chu and J. A. Mulder Nonlinear Flight Control Design Using Constrained Adaptive Backstepping *Journal of Guidance, Control, and Dynamics*, vol. 30, no. 2, pp. 322–336, 2007, doi: 10.2514/1.25834.
- [14] Q. Hu, Y. Meng, C. L. Wang and Y. M. Zhang Adaptive Backstepping Control for Air-breathing Hypersonic Vehicles with Input Nonlinearities *Aerospace Science and Technology*, vol. 73, pp. 289–299, 2018, doi: 10.1016/j.ast.2017.12.001.
- [15] R. S. Sutton and A. G. Barto *Reinforcement Learning: An Introduction*. 6th edition, Sigma Series in Pure Mathematics. Cambridge, MA, USA: A Bradford Book, 2018.
- [16] Y. Zhou, E. van Kampen and Q.P. Chu Incremental Model Based Online Dual Heuristic Programming for Nonlinear Adaptive Control *Control Engineering Practice*, vol. 73, pp. 13–25, 2018, doi: 10.1016/j.conengprac.2017.12.011.
- [17] Y. Zhou, E. van Kampen and Q. P. Chu Incremental Approximate Dynamic Programming for Nonlinear Flight Control Design In *Proceedings of the EuroGNC 2015*, Toulouse, France, 2015.
- [18] Y. Zhou, E. van Kampen and Q. P. Chu Incremental Approximate Dynamic Programming for Nonlinear Adaptive Tracking Control with Partial Observability *Journal of Guidance, Control, and Dynamics*, vol. 41, no. 12, pp. 2554–2567, 2018, doi: 10.2514/1.G003472.
- [19] Y. Zhou, E. van Kampen and Q.P. Chu An Incremental Approximate Dynamic Programming Flight Controller Based on Output Feedback *AIAA Guidance, Navigation, and Control Conference*, San Diego, California, USA, January, 2016, doi: 10.2514/6.2016-0360.
- [20] B. Sun and E. van Kampen Incremental Model-Based Heuristic Dynamic Programming with Output Feedback Applied to Aerospace System Identification and Control *2020 IEEE Conference on Control Technology and Applications*, Montreal, QC, Canada, 2020, pp. 366-371, August, 2020, doi: 10.1109/CCTA41146.2020.9206261.
- [21] B. Sun and E. van Kampen Intelligent Adaptive Optimal Control Using Incremental Model-Based Global Dual Heuristic Programming Subject to Partial Observability *Applied Soft Computing*, vol. 103, pp. 1–15, 2021, doi: 10.1016/j.asoc.2021.107153.
- [22] B. Sun and E. van Kampen Reinforcement-Learning-Based Adaptive Optimal Flight Control with Output Feedback and Input Constraints *Journal of Guidance, Control, and Dynamics*, vol. 44, no. 9, pp. 1685–1691, 2021, doi: 10.2514/1.G005715.
- [23] B. Sun and E. van Kampen Event-Triggered Constrained Control Using Explainable Global Dual Heuristic Programming for Nonlinear Discrete-Time Systems *Neurocomputing*, vol. 468, pp. 452–463, 2022, doi: 10.1016/j.neucom.2021.10.046.
- [24] Y. Zhou, E. van Kampen and Q.P. Chu Incremental Model Based Heuristic Dynamic Programming for Nonlinear Adaptive Flight Control In *Proceedings of the International Micro Air Vehicles Conference and Competition*, Beijing, China, October, 2016, url: <https://www.imavs.org/papers/2016/25.pdf>.
- [25] Y. Zhou, E. van Kampen and Q. P. Chu Incremental Model based Online Heuristic Dynamic Programming for Nonlinear Adaptive Tracking Control with Partial Observability *Aerospace Science and Technology*, vol. 105, pp. 1–14, 2020, doi: 10.1016/j.ast.2020.106013.
- [26] S. Heyer, D. Kroezen and E. van Kampen Online Adaptive Incremental Reinforcement Learning Flight Control for a CS-25 Class Aircraft *AIAA Scitech 2020 Forum*, Orlando, FL, USA, October, 2020, doi: 10.2514/6.2020-1844.
- [27] L.G. Sun, C.C. de Visser, Q.P. Chu and W. Falkena Hybrid Sensor-Based Backstepping Control Approach with Its Application to Fault-Tolerant Flight Control *Journal of Guidance, Control, and Dynamics*, vol. 31, no. 1, pp. 59–71, 2014, doi: 10.2514/1.61890.
- [28] Y. Zhou, E. van Kampen and Q.P. Chu Launch Vehicle Adaptive Flight Control with Incremental Model Based Heuristic Dynamic Programming *International Astronautical Congress*, Adelaide, Australia, September, 2017.
- [29] S. Mysore, B. Mabsout, R. Mancuso and K. Saenko Regularizing Action Policies for Smooth Control with Reinforcement Learning *IEEE International Conference on Robotics and Automation*, Xi'an, China, October, 2021, doi: 10.1109/ICRA48506.2021.9561138.
- [30] A.N. Kalliny, A.A. El-Badawy and S.M. Elkhamsy Command-Filtered Integral Backstepping Control of Longitudinal Flapping-Wing Flight *Journal of Guidance, Control, and Dynamics*, vol. 41, no. 7, pp. 1556–1568, 2018, doi: 10.2514/1.G003267.
- [31] J.A. Farrell, M. Polycarpou, M. Sharma and W. Dong Command Filtered Backstepping *IEEE Transactions on Automatic Control*, vol. 54, no. 6, pp. 1391-1395, 2009, doi: 10.1109/TAC.2009.2015562.
- [32] R.A. Hull, D. Schumacher and Z.H. Qu Design and Evaluation of Robust Nonlinear Missile Autopilots from a Performance Perspective In *Proceedings of 1995 American Control Conference*, Seattle, WA, USA, June, 1995, doi: 10.1109/ACC.1995.529235.
- [33] P. J. Werbos Advanced Forecasting Methods for Global Crisis Warning and Models of Intelligence *General Systems*, vol. 22, pp. 25-38, 1977, url: <https://gwern.net/doc/reinforcement-learning/1977-werbos.pdf>.
- [34] K. Shibata Dynamic Reinforcement Learning for Actors *arXiv preprint*, 2025, doi: 10.48550/arXiv.2502.10200.
- [35] B. Sun and E. van Kampen Incremental Model-Based Global Dual Heuristic Programming with Explicit Analytical Calculations Applied to Flight Control *Engineering Applications of Artificial Intelligence*, vol. 89, pp. 103425, 2020, doi: 10.1016/j.engappai.2019.103425.